PORTIO

OF TH

DOCUM

ARE

ILLEGIB

27C
4-20-81

Dr. 2536

R-3679

ornl

ORNL-5690

MASTER

OAK RIDGE NATIONAL LABORATORY

UNION CARBIDE

Development of Variable-Width Ribbon Heating Elements for Liquid-Metal and Gas-Cooled Fast Breeder Reactor Fuel-Pin Simulators

R. W. McCulloch
D. W. Post
R. T. Lovell
S. D. Snyder

OPERATED BY
UNION CARBIDE CORPORATION
FOR THE UNITED STATES
DEPARTMENT OF ENERGY

ORNL-5690
Dist. Category UC-77,
UC-79, -79e, -79p

Contract No. W-7405-eng-26

Engineering Technology Division

DEVELOPMENT OF VARIABLE-WIDTH RIBBON HEATING ELEMENTS FOR LIQUID-METAL AND GAS-COOLED FAST BREEDER REACTOR FUEL-PIN SIMULATORS

R. W. McCulloch   R. T. Lovell
D. W. Post   S. D. Snyder

Date Published: April 1981

Prepared by the
OAK RIDGE NATIONAL LABORATORY
Oak Ridge, Tennessee 37830
operated by
UNION CARBIDE CORPORATION
for the
DEPARTMENT OF ENERGY

CONTENTS

LIST OF FIGURES

ACKNOWLEDGMENTS

This effort was successfully completed because of the close coordination of five divisions of the Oak Ridge National Laboratory (ORNL) and the Y-12 Plant: the ORNL Engineering Technology Division and Metals and Ceramics Division, and the three Y-12 divisions of Development, Fabrication, and Assembly. Guidance and support were provided by M. H. Fontana, the Breeder Reactor Program Manager, and Uri Gat, the Gas-Cooled Fast Breeder Reactor Program Manager.

Dave Clark first understood the need for a variable-width ribbon heating element. The first analytical work for such a ribbon, wound from a strip, was done by Tom Kress. However, many innovations were needed to transform the material from a rectangular sheet to a precisely wound heating element with a chopped-cosine heat flux distribution. John Hurst, Y-12 Fabrication Division, was the first to realize that precise contours could be achieved with a template grinding machine. Ray Carter, C. B. Cliff, B. J. Hill, and J. T. Forrester installed most of the fixtures and made template grinding a viable process. H. A. Hutcheson, L. A. Meade, C. K. Endsley, and J. H. Wiley, winding Foreman of the Y-12 Assembly Division, were responsible for much of the tooling, fixture installment, and winding innovations necessary to wind a continuously variable strip into a coil. Dick Heestand of the ORNL Metals and Ceramics Division solved many of the original problems encountered in final processing and cleaning of the wound coils. Finally, Ralph Dial and Ken Finnell of the ORNL Engineering Technology Division determined and completed the final critical steps necessary for the coils to become an active part of a fuel pin simulator.

A special acknowledgment is extended for the valuable contributions of R. E. MacPherson, Manager, Experimental Engineering Section, Engineering Technology Division, for his support and guidance throughout the development of this project and during the writing, editing, and reviewing of this report.

DEVELOPMENT OF VARIABLE-WIDTH RIBBON HEATING ELEMENTS FOR LIQUID-METAL AND GAS-COOLED FAST BREEDER REACTOR FUEL PIN SIMULATORS

R. W. McCulloch   R. T. Lovell
D. W. Post   S. D. Snyder

ABSTRACT

Variable-width ribbon heating elements that provide a chopped-cosine variable heat flux profile have been fabricated for fuel pin simulators used in test loops by the Breeder Reactor Program Thermal-Hydraulic Out-of-Reactor Safety test facility and the Gas-Cooled Fast Breeder Reactor—Core Flow Test Loop.

Thermal, mechanical, and electrical design considerations are used to derive an analytical expression that precisely describes ribbon contour in terms of the major fabrication parameters. These parameters are used to generate numerical control tapes that control ribbon cutting and winding machines. Sixty ribbons are cut, 15 at a time, by a template grinding machine from one assembly of 15-cm-wide (6-in.) strips, stacked 15 high. A staging technique is developed to allow cutting of ribbon lengths longer than 137 cm (54 in.). Local width and total ribbon contour tolerances are routinely held to within ±0.5% during cutting. The ribbons are then wound into a coiled helix, closely approximating the dimensions needed for later use. Final touch-up swaging sets the coil diameter, length, gaps, surface finish, and mechanical condition to the precise tolerances required.

Infrared scanning techniques are developed to determine the optimum transient thermal profile of the coils and relate this profile to that generated by the coils in completed fuel pin simulators.

---

1. INTRODUCTION

Nuclear fuel pin simulators (FPSs or pins) are necessary to the operation of thermal-hydraulic test facilities for four Oak Ridge National Laboratory (ORNL) programs: (1) the Blowdown Heat Transfer—Thermal-Hydraulic Test Facility (BDHT—THTF), (2) the Gas-Cooled Fast Breeder Reactor—Core Flow Test Loop (GCFR—CFTL), (3) the Breeder Reactor Program Thermal-Hydraulic Out-of-Reactor Safety (BRP-THORS) Facility, and (4) the Multirod Burst Test (MRBT) program and test facility. These experimental facilities are used to conduct out-of-reactor thermal-hydraulic and mechanical interaction safety tests for both light-water and breeder reactor programs. The FPS units simulate the geometry, heat flux profiles, and operational capabilities of a reactor core element under steady-state and transient conditions. During transient tests, FPSs are subjected to temperatures as high as 1375°C (2500°F), power levels as high as 57.5 kW/m (17.5 kW/ft), and severe thermal stress.

The heat flux profile for an FPS is generated by passing an electric current through a tubular or coiled ribbon heating element embedded in boron nitride (BN) insulation within its stainless steel sheath. "Chopped-cosine" (cosi profile chopped at either end so that power goes to zero abruptly) heat flux profiles for BRP-THORS and GCFR-CFTL FPSs have been generated previously by varying the helical pitch of a constant-width ribbon. While acceptable for steady-state tests, this method caused unacceptable transient heat flux profile perturbations. A thorough summary of development in support of the BRP program is presented in Ref. 1.

This report describes the design, fabrication development, and inspection of variable-width, helically wound heating elements for the BRP and GCFR programs; these elements eliminate the disadvantage of variable-pitch ribbons, while providing other important advantages to an evolving FPS fabrication technology.

2. FUEL PIN SIMULATOR DESCRIPTION

Variable-width ribbon heating elements were developed for the BRP-THORS FPS and the GCFR-CFTL FPS. While they are similar in many respects, major differences exist in the purpose, design, and operation of the two simulators.

Intended for use in a liquid sodium environment, the BRP FPS (Fig. 2.1) has a double-ended design (current enters one end and exits the other) with a 5.84-mm-OD (0.230-in.) by 0.38-mm-thick (0.015-in.) clad. The 3.175-mm-OD (0.125-in.) heating element has a total resistance of 3.039 Ω, a peak-to-average heat flux ratio of 1.30:1, and a peak-to-minimum ratio of 2.92:1. The BN preforms provide structure and insulation in the central and annular regions and three 0.38-mm (0.015-in.) type K, insulated-junction thermocouples (TCs) (with BN substituted for magnesium oxide in the junction region) are located at 120° intervals and various axial locations within the FRS annular region. One end of the variable-width ribbon is connected to the power supply via a nickel intermediate rod which, in turn, is joined to a copper rod. The ground connection is made by welding the nickel ground plug to the ground lead extension which, in turn, is welded to the stainless steel (SS) clad.

Power is obtained by I^2R heating of the ribbon. The FPS is capable of operating at a peak heat flux of 400 W/cm^2 (55 kW/m, 390 V at 130 A) at 1000°C (1832°F) clad temperature for short periods of time and at 315 W/cm^2 (43.3 kW/m) at 1000°C indefinitely. Additionally, the FPS is designed to withstand sodium voiding and clad dryout for 1 s while operating at 315 W/cm^2 (43.3 kW/m) at 1000°C (1832°F). Eight bundles of FPSs in 13 different configurations have been assembled and tested under various operational conditions in the THORS facility.[2,3]

During FPS assembly, BN performs are inserted and individually crushed inside the heating element while the coil and terminals are encased in a rigid containment enclosure. This heating element assembly is then positioned within the instrumented SS clad, and the annular BN insulation is inserted in a manner similar to that employed with central preforms. The entire FPS is then swaged to the final size. The swaging operation provides final compaction of the insulation so that the density

ORNL-DWG 79-5320 ETD

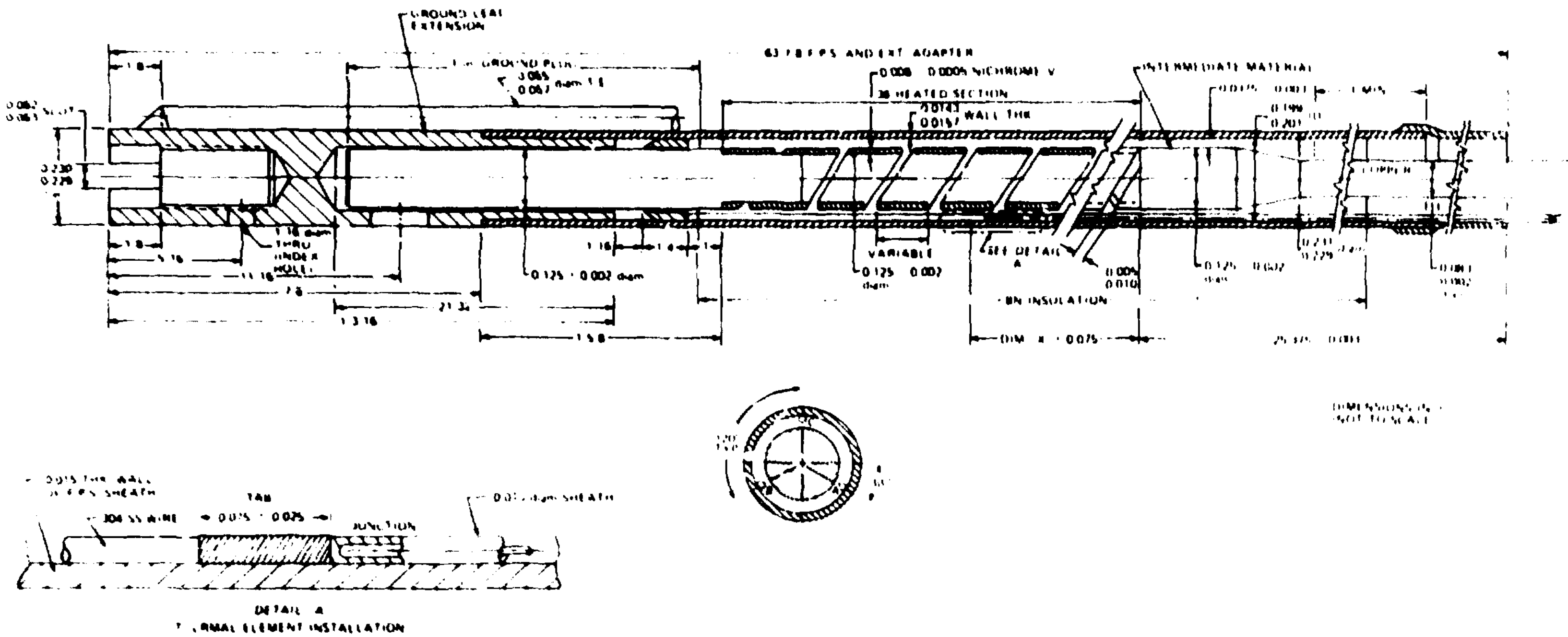

Fig. 2.1. Breeder Reactor Program fuel pin simulator (FPS).

is ~2.14 g/cm^3 (95% theoretical density) and the coil is in intimate contact with the insulation.

The GCFR–CFTL FPS (Fig. 2.2) is larger in diameter than the BRP-THORS FPS (8.0 mm diam) and is single-ended in configuration (current enters and exits through the same end). The SS clad is roughened in the region adjacent to the heated length to enhance heat transfer to a flowing helium environment. External power is supplied to the 4.76-mm-OD (0.1875-in.) variable-width ribbon heating element via nickel-to-copper tubular terminals and returned via a nickel central rod brazed to a copper central terminal. The BN insulation is contained in annular regions internal and external to the heating element and terminals. The coil has a resistance of 2.5 Ω, a peak-to-average heat flux ratio of 1.21:1, and a peak-to-minimum ratio of 2.0:1. Six 0.5-mm (0.020-in.) insulated-junction type K TCs are contained within the external annular region at 60° circumferential and various axial locations.

The FPS is designed to operate at a peak heat flux of 200 W/cm^2 (50.3 kW/m, 342 V at 127 A) at 1000°C (1832°F) clad temperatures and up to clad melting (1375°C) at 40 W/cm^2 (8.3 kW/m).

The CFTL FPS is fabricated similarly to the THORS FPS except that it uses a newly developed "nonswaged" fabrication process. In this process, BN preforms have been designed and fabrication techniques developed so that intimate contact between the heating element, clad, and BN insulation is ensured and, at the same time, relatively high thermal conductivity is achieved in the BN without swaging the unit. This process enables prototypal GCFR-roughened cladding to be used (swaging would distort the external clad roughening). A summary of the FPS development efforts to date is provided in Refs. 4 and 5.

Without the variable-width ribbon heating element, a variable-profile FPS using advanced BN preform fabrication techniques could not have been fabricated. To obtain a chopped-cosine heat flux distribution with a constant-width ribbon, the gap must be varied between turns. When the gap becomes larger than ~1 mm (0.039 in.), the coiled ribbon will no longer contain the BN insulation that is installed in the coil and crushed as the first step in the assembly operation. The use of variable-width ribbon heating elements allows the gap to be relatively constant along

ORNL-DWG 80-5963 ETD

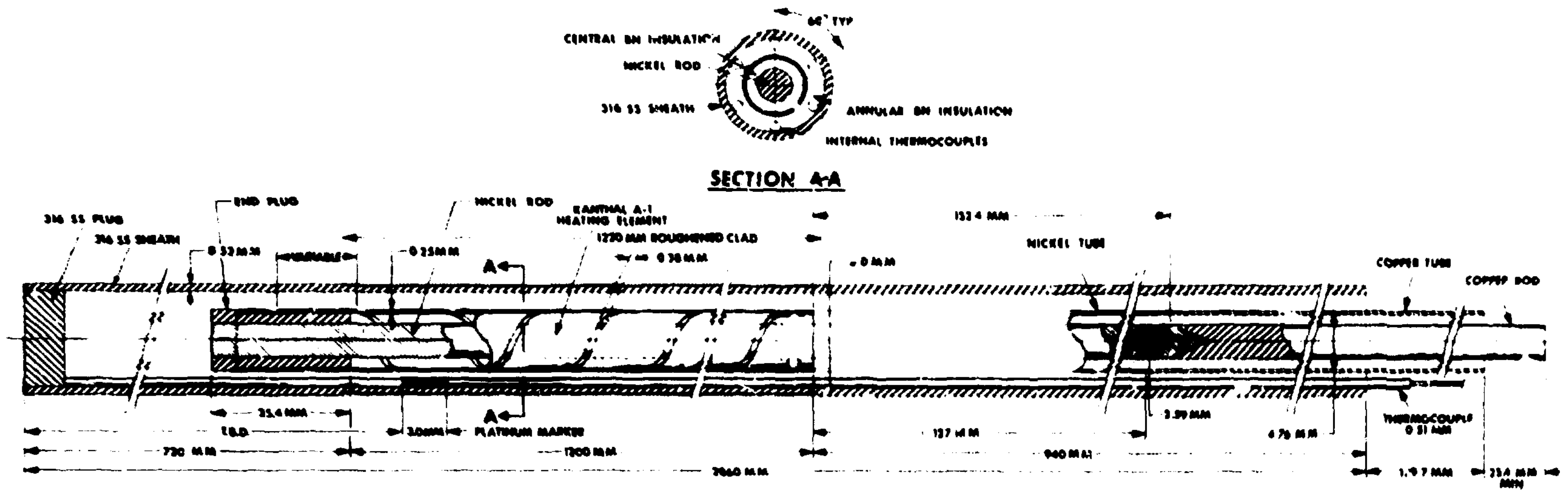

Fig. 2.2. Gas-Cooled Fast Breeder Reactor—Core Flow Test Loop (GCFR—CFTL) fuel pin simulator.

the length of the coil, and FPSs have been fabricated with a gap width of no more than 0.25 mm (0.010 in.).

8

3. VARIABLE-WIDTH RIBBON HEATING ELEMENT DESIGN

3.1 General

As the power-generating component of an FPS, the heating element is required to operate under conditions approaching the maximum capability of the material. As such, the design must include careful consideration of the thermal, mechanical, and electrical properties of the material as well as the FPS physical dimensions. Careful attention to heating element design can extend the operating range or lifetime of an FPS considerably.

3.2 Thermal-Mechanical Design

A high heat flux FPS may have a radial temperature profile as high as 300°C/mm so that the radial distance from clad outside diameter to heating element inside diameter directly determines maximum operating conditions for a given clad temperature and heating element material. As a general rule, the coiled heating element diameter should (1) be as large as possible consistent with maintaining an appropriately thick BN annular insulation region that will contain FPS internal TCs, (2) maintain acceptable insulation resistance at the maximum required operational temperatures, and (3) withstand the required clad to heating element voltage potential without dielectric breakdown.

The heating element should be as thin as practical because the FPS peak internal temperature will increase as the ribbon thickness is increased (for a constant outside diameter). However, this is balanced by several other considerations. Problems in forming or fabricating the ribbon place practical limits on the minimum ribbon thickness. For Nichrome V and Kanthal A-1 material, this limit is 0.2 mm (0.008 in.), but it is 0.15 mm (0.006 in.) for the Pt-8% W ribbon material. Handling, assembling, and swaging of ribbons and FPSs also dictate a minimum ribbon thickness; the limits previously established are compatible with these operations. As the ribbon thickness decreases, the percent variation in thickness becomes much harder to control. This, in turn, affects local heat generation because local power generation (constant current through the ribbon) is inversely proportional to thickness. A practical tolerance limit for ribbon thickness is 0.0125 mm (0.0005 in.). This represents a local power variation of 2.5% for a 0.5-mm-thick (0.020-in.) ribbon, but this variation is doubled for the 0.25-mm (0.10-in.) ribbons common to this effort. Finally, the heating element must be capable of withstanding differential thermal expansion without permanent deformation during transient tests.

Because transient operation of FPSs in both BRP-THORS and GCFR-CFTL programs is of paramount concern, the heating element configuration must be carefully analyzed under transient conditions to determine performance. Heat capacity effects become pronounced in the transient heat flux profile, and axial conduction does not smooth out the profile as it does under steady-state conditions. Further, with the use of BN preform technology, axial conduction is much lower than radial conduction because of the anisotropic nature of thermal conductivity in BN preforms. Thus, under transient conditions, such properties as turn-to-turn spacing (which affects the ratio of heated to nonheated surface as discussed in the following section), coil diameter variations, coil turns per inch, and eccentricity of the heating element become important.

The term "surface ratio," the ratio of external surface area of the heating element to the surface area of a cylinder having the same outside diameter, is used to quantify the heat flux uniformity of a given heating element design. Thus, the surface ratio of a tubular heating element would be 100%. The surface ratio of an FPS heating element should be above 90%. To keep the surface ratio above 90% requires minimal spacing between turns of a helical coil, but because the volts per turn are quite small (almost always <1 at normal operating conditions), there is little chance of short circuiting between turns in a well-made heating element. The chance of the turns physically touching is also small, if the recommended methods of fabrication are followed.

Coil diameter variations are important because the clad surface transient heat flux is locally increased if the local coil diameter increases. Heat flux is increased because a decreased radial gap provides a shorter path for heat conduction and the annular volumetric heat storage capacity is decreased while the local steady-state and transient heat generation is increased (because there is more ribbon per turn in a larger-diameter coil). Conversely, a smaller diameter decreases local clad surface heat flux.

Similarly, coil eccentricity results in a disturbance of the circumferential heat flux profile. Using the Heating V code, calculations of these coil variations indicate that a 0.025-mm-diam (0.001-in.) change or eccentricity results in 1% perturbation of the transient heat flux profile.

3.3 Electrical Design

Evaluation of thermal, mechanical, and physical properties will provide reasonable design limits for the variable-width coil and ensure that it will be both fabricable and suitable to its environment. However, electrical considerations provide the design basis for the exact configuration to meet FPS operational requirements.

To a great degree, design of the heating element itself is dependent on the available power supply, which can be expected to have maximum values of available current and voltage. Assuming that each FPS will be connected to the available voltage, the current must be divided among the number of FPSs in the bundle to arrive at the maximum value for each FPS. (In some installations with single-ended heater designs, the use of various series-parallel arrangements may be advantageous.)

From the maximum available voltage, the maximum value for heating element resistance (R) at operating temperature can be calculated from the equation

$$R = V^2/W ,$$

where V is voltage and W is watts. From the maximum available current, the minimum value for heating element resistance at operating temperature can be calculated from the formula

$$R = W/I^2 ,$$

where I is current. A "window" (or spread) can be established for the heating element resistance from these two values. A resistance value well within this window should be selected to allow for subsequent variations that could occur in volume resistivity, physical sizes, and fabrication techniques. Within a particular number of FPS units made from the same lots of material, variations in total resistance should be kept to less than ±2% to ensure minimum pin-to-pin power variation in a bundle.

Where capability of the power supply permits (or where a power supply is to be specified), some compromise should be made between current and voltage ratings. The major consideration in both GCFR and BRP FPSs was to limit current to prevent excessive heating of the lead-in sections, as well as the leads themselves, and to simplify connection problems that can be significant in larger bundles. However, the voltage is kept low to decrease the chance of developing short circuits or, alternately, to allow the annular insulation gap to be as small as possible. Although no exact rule has been established, recommendations are that a resistance between 1 and 3 Ω be used for small-diameter FPSs. Because of terminal heating problems in both BRP and GCFR FPSs and because advances in FPS fabrication technology have enabled the maximum applied voltage across the insulation gap to increase to ~350 V (600 V/mm), both BRP and GCFR variable-width ribbon heating elements have been designed with the coil resistance between 2.5 and 3 Ω.

This value is the "cold" or room temperature resistance. The temperature coefficient of resistivity (TCR) of heating element material must also be known because the "hot" resistance is 6 to 10% higher than the cold resistance. The resistance value of the heating element at ~1000°C is normally used in design calculations because this is a common use temperature and very little change in resistance occurs in the 800 to 1200°C range (at least in Nichrome and Kanthal materials).

Consideration of the ribbon resistance change in winding, swaging, and FPS swaging should be factored in if the window is <10% of total ribbon resistance. Average resistance will increase about 1% when the ribbon is wound and swaged on a mandrel. If the FPS is swaged, a 5 to 7% decrease in resistance will occur because of ribbon thickening. When a swaged FPS is annealed, another ~5% drop will occur, making a total decrease of about 10 to 12%. However, for resistances within the window established by the FPS power, power supply, and other considerations, the absolute value is not nearly as critical as the variation in resistance from ribbon to ribbon. This variation should be maintained as low as possible, with ±2% as a reasonable tolerance limit.

Once the ribbon resistance has been determined, factors describing the FPS power profile are needed:

1. peak/average power, P_p/P_a;
2. peak/minumum power, P_p/P_m; and
3. axial heated length, C.

Other information obtained from the overall FPS design is also necessary:

1. heating element material resistivity, ρ;
2. ribbon thickness, t; and
3. coiled ribbon pitch diameter, $D = OD - t$.

The local widths of an axial length of ribbon, C, may now be calculated in terms of resistance, using the method of Fig. 3.1.

Optimization of the various parameters is an iterative process that must be accomplished with these principles in mind. An additional recommendation is that the minimum ribbon width be at least five times its thickness to reduce handling and winding problems. Theoretically, the width can be as great as the coil circumference based on its pitch diameter D (in which case the ribbon becomes a tube). However, for coiled ribbon, recommendations are that the winding angle θ be no less than 45° and the width be no more than 70.7% of the pitch diameter.

To provide a high surface ratio, spacing between turns of the ribbon should be minimal. While no general rule has been established, a minimum value of 0.25 mm (0.010 in.) in the completed FPS is recommended. To provide reasonably uniform surface heat flux, this spacing should never be greater than the combined thickness of the BN insulation and the FPS sheath. Spacing greater than that recommended can produce significant peaks and valleys in the surface heat flux.

Equations (3.1) through (3.7) in Fig. 3.1 derive a relationship for the width w of a constant-width ribbon in terms of the input variables mentioned previously. Implicit in the derivation is a turn-to-turn spacing G of zero (i.e., the coil is wound with turns touching). The

ORNL-DWG 80-5573A ETD

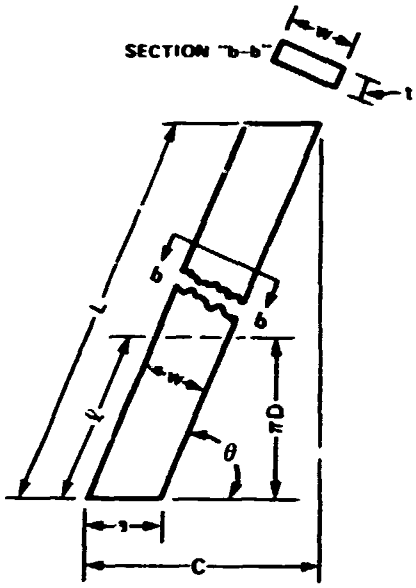

Definitions

θ = winding angle

w = width of heating element

t = thickness of heating element

a = axial length of width

C = axial length of heating element

1/a = turns per cm

ℓ = length of ribbon for 1 turn

L = overall length of ribbon

N = number of turns in coil

D = pitch diameter of coil

A = cross-sectional area of ribbon

R = resistance of heating element

Equations, Derivations, and Calculations

(3.1) $\sin\theta = \frac{\pi D}{\ell} = \frac{w}{a}$

(3.2) $\cos\theta = \frac{a}{\ell} = \frac{w}{\pi D}$

(3.3) $\frac{1}{a} = \frac{\sin\theta}{w}$

(3.4) $N = \frac{C}{a} = \frac{C\sin\theta}{w} = \frac{C}{\pi D}\tan\theta$

(3.5) $L = N\ell = \frac{C}{\ell\cos\theta}\cdot\ell = \frac{C}{\cos\theta}$

(3.6) $A = \frac{\rho L}{R} = \frac{\rho C}{R\cos\theta} = \frac{\pi D\rho C}{Rw}$

(3.7) $w = \frac{A}{t} = \frac{\pi D\rho C}{Rtw} = \left(\frac{\pi D\rho C}{Rt}\right)^{1/2}$

Fig. 3.1. Design of rectangular ribbon heating element.

unstretched length should be 90 to 95% of the final length. If the FPS is to be swaged, the elongation of the unit and the resultant increase in turn spacing must also be considered.

If a constant-width coil is to be designed, Eq. (3.7) can be used with values of t and D adjusted to optimize w. Equations (3.2), (3.3), and (3.4) are then used to calculate the winding angle θ, the turns per centimeter 1/a, and the total turns N, respectively. Standard values for t listed in heating element vendor catalogs should be used. Recommendations are that several calculations be made before a final design is determined.

To calculate the width of a variable-width ribbon, similar procedures are followed except that calculations are made for a peak resistance per unit length R_p of the wound ribbon at the center of the cosine profile (Fig. 3.2). For this condition, R_p is given by

$$R_p = (R/C)(P_p/P_a)\Omega/\mathrm{cm} .$$

To modify Eq. (3.7) to enable calculation of the ribbon width w_p at the center of the profile, R is replaced by R_p and C is understood to be 1 cm, so that w_p is given by

$$w_p = \left(\frac{\pi D\rho}{R_p t}\right)^{1/2} . \tag{3.7a}$$

ORNL-DWG 80-5572A ETD

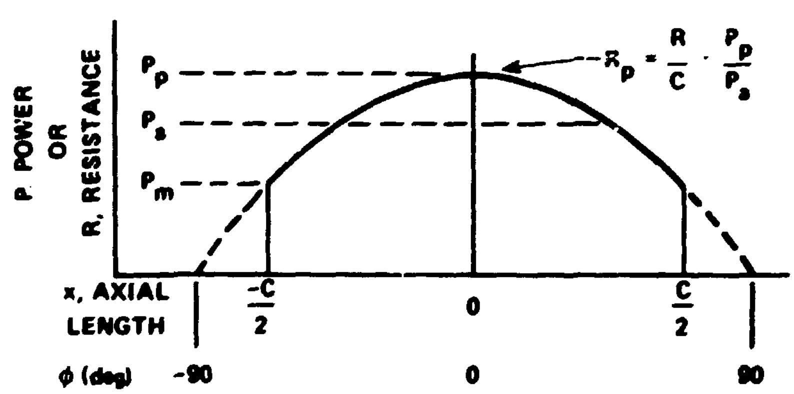

Fig. 3.2. Variable heat flux power profile.

Similarly, Eqs. (3.2) and (3.3) become

$$\theta_p = \cos^{-1}(w_p/\pi D) \tag{3.2a}$$

and

$$1/a_p = \sin \theta_p/w_p \ . \tag{3.3a}$$

The value of N can be determined using Eq. (3.4) and the average winding angle, θ_a, determined from Eq. (3.13). Thus,

$$N = \frac{C}{\pi D} \tan \theta_a \ . \tag{3.4a}$$

This sequence for design of a variable-width ribbon is summarized in Table 3.1. The various input parameters are entered in items 2 through 8.

Table 3.1. Ribbon heating element design sheet

Item	Parameter	BRP coil	GCFR coil
1	Desired resistance R, Ω	3.04	2.50
2	P_p/P_m	2.92	2.00
3	P_p/P_a	1.30	1.21
4	Coil axial length C, cm	83.82	107.95
5	Stretched length, cm	87.63	113.03
6	Ribbon thickness t, cm	0.254	0.254
7	Pitch diameter D, mm	2.921	4.00
8	Material resistivity ρ, $(\Omega - \mathrm{cm}) \times 10^{-6}$	144.9078	144.9578
9	$R_p = (1 \cdot 3)/4$, Ω/cm	0.04715	0.02802
10	$w_p = \left(\frac{\pi \cdot 7 \cdot 8}{9 \cdot 6}\right)^{1/2}$, cm	0.33328	0.50589
11	$\theta_p = \cos^{-1}\left(\frac{10}{\pi \cdot 7 \cdot 10^{-1}}\right)$, deg	68.70	66.26
12	$N = \frac{(4) \cdot}{\pi \cdot (7) \cdot 10^{-1}} \tan \left\{\cos^{-1}\left[(3)^{1/2} \cdot \cos(11)\right]\right\}$, turns	200.7	173.92
13	$g = \frac{(5 - 4)}{12 \cdot 10^{-1}}$, mm	0.195	0.286

Values for R_p, w_p, θ_p, and N are then calculated from the input parameters. The gap width between turns for the stretched coil is then calculated in item 13. An example of calculations for the BRP coil (design 1) and the GCFR coil (design 2) are given in the table.

The design of a ribbon profile to give a specific axial heat flux distribution was first reported by D. L. Clark and T. S. Kress.[6] The local heat flux distribution was established from the following relation:

$$P = \frac{I^2\rho}{w^2t} , \tag{3.8}$$

where P is the local power per unit area, w is the local ribbon width, and I is the current.

Solving Eq. (3.8) for the local ribbon width w gives

$$w = \left(\frac{I^2\rho}{Pt}\right)^{1/2} . \tag{3.9}$$

If we use Eq. (3.9) to define the power at some reference position, such as the center where $P = P_p$ and $w = w_p$, then the local width w with respect to the reference width is

$$w = \left(\frac{P_p}{P}\right)^{1/2} w_p . \tag{3.10}$$

Equation (3.10) can be used to establish relative width anywhere along the ribbon. However, knowing just the width is not sufficient. The ribbon must be wrapped around a mandrel to form the coil of the desired length L and diameter. Figure 3.3(a) shows the uncoiled ribbon contour, and Fig. 3.3(b) shows the coiled configuration. For the coil to wind properly, the slope of the contour θ must be the same at any position along the abcissa [Fig. 3.3(a)] on both sides of the ribbon. Thus, the vertical component of the ribbon width w_v for the gap $G = 0$ is constant [Fig. 3.3(a)]:

$$w_v = \pi D , \tag{3.11}$$

where D is the ribbon pitch diameter as defined previously. The local

ORNL-DWG 80-5574A ETD

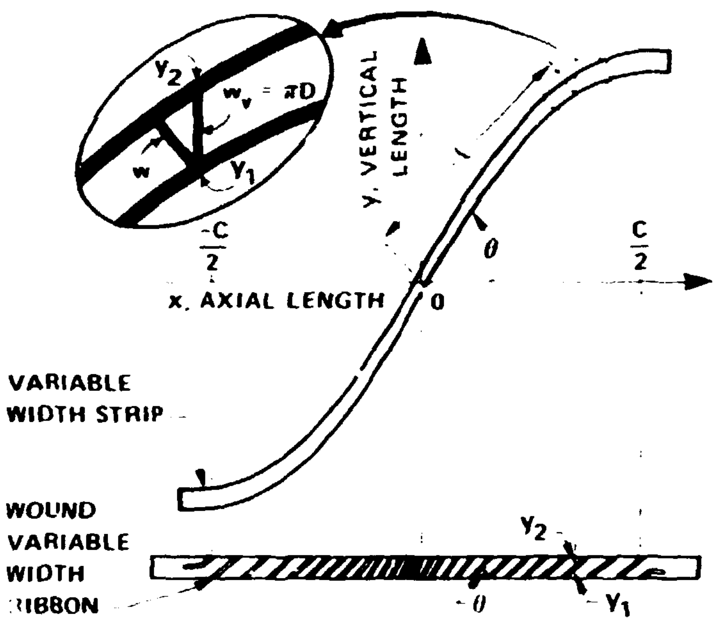

Fig. 3.3 Variable-width ribbon (a) before and (b) after being wound into coil.

width w is given in terms of the contour angle θ by

$$w = \pi D \cos \theta \ , \tag{3.12}$$

or in terms of a reference angle θ_p at P_p and w_p by

$$\cos \theta = \left(\frac{P_p}{P}\right)^{1/2} \cos \theta_p \ . \tag{3.13}$$

Referring again to Fig. 3.3(a), the ribbon contour in the x,y plane can now be completely defined by x, y, θ, and w. The chopped-cosine power profile is conveniently defined in terms of the ribbon length such that $P = P_p$ at $x = 0$ and $P = P_m$ at $x = \pm C/2$.

Referring to Fig. 3.2, the power profile can be defined by

$$P = P_p \cos \phi \ , \tag{3.14}$$

where ϕ is the angle that relates the power profile to the wound-ribbon axial length C. By definition, $\cos \phi_p = P_p/P_p = 1$ and $\phi_p = 0°$ at P_p. The angle at P_m where $x = \pm C/2$ is now

$$\phi_m = \cos^{-1}\left(\frac{P_m}{P_p}\right) . \tag{3.15}$$

So the profile can be described within the chopped region by

$$\frac{P}{P_p} = \cos \phi = \cos \left[\left(\cos^{-1} P_m/P_p\right) \frac{2x}{C}\right] . \tag{3.16}$$

The vertical contour or winding angle θ can now be determined in terms of the specific profile information by substitution of Eq. (3.16) into Eq. (3.13):

$$\cos \theta = \left\{\frac{1}{\cos \left[(\cos^{-1} P_m/P_p) \frac{2x}{C}\right]}\right\}^{1/2} \cos \theta_p . \tag{3.17}$$

Local width w is then calculated using Eq. (3.12), which defines the ribbon contour in terms of θ and w at any x for $-C/2 \leq x \leq C/2$.

The final task is then to determine ℓ and y in terms of x for a given ribbon contour and compile the information in a form amenable to the generation of magnetic tapes for numerically controlled (NC) ribbon machining and winding.

From Fig. 3.3(a),

$$\ell = \frac{x}{\cos \theta} , \tag{3.18}$$

and

$$y = x \tan \theta . \tag{3.19}$$

A program written for an HP-25C programmable calculator computes sin θ, w, ℓ, and y in terms of x in increments of $x = 1$ cm. Equations (3.17), (3.12), (3.18), and (3.19), respectively, were modified as shown:

$$\cos \theta_n = \left\{ \frac{1}{\cos\left[(\cos^{-1} P_m/P_p)\right]\frac{2x_n}{C}} \right\}^{1/2} \cos \theta_p \ , \tag{3.20}$$

$$w_n = w_v \cos \theta_n \ , \tag{3.21}$$

$$\ell_n = \ell_{n-1} + \frac{x_n}{\cos \theta_n} \ , \tag{3.22}$$

$$y_n = y_{n-1} + x_n \tan \theta \ . \tag{3.23}$$

The contour is calculated for $0 \leq x \leq C/2$ because the coil is symmetric about the $x,y = 0$ position.

In summary, the design sheet (Table 3.1) is used to determine θ_p and w_p from the given ribbon design information. Sin θ_p, the chopped-cosine profile information (P_m/P_p), and the ribbon-wound length (C) are then used in Eqs. (3.20) through (3.23) to derive the specific x,y profile data needed for NC machining and winding.

4. HEATING ELEMENT CONTOUR MACHINING

4.1 General

The objective of the machining phase of ribbon development was to take the ribbon contour information and fabricate ribbons of variable width having a precisely controlled contour. The major requirement was to hold the variation in the calculated width to <1% throughout the entire ribbon length. Additionally, the x and y locations describing the exact placement of the ribbon on the x,y plane (and therefore the angle) were to be held to within 1%. Proper ribbon local tolerances are important, but displacement of y_1, y_2 values for a given x value (with the width in tolerance) are just as detrimental to ribbon winding as are width variations.

Early attempts to machine the ribbon contour on an NC end-milling machine were unsuccessful because these tolerances could not be held and excessive ribbon-edge burring occurred. Abrasive machining or grinding utilizing the "sandwich" technique (discussed below) was then attempted.

Tooling and fixtures were designed and fabricated to allow up to four stacks of elements to be machined from a single stack of ribbon raw material, thus saving tooling and machining time. A second major problem of machine travel limitation was solved by using a staging technique to extend the machine range from 137 to ~245 cm (54 to 96.5 in.), thus providing adequate travel for both GCFR and BRP element machining. Final production techniques allowed machining of 4 stacks of 15 elements each for a total of 60 elements per operation. Width and contour tolerances have been held to less than ±0.5% variation.

The template grinding machine, the method of generating and using the NC drive tape, and the development of the fabrication process are discussed in the following sections.

4.2 Template Grinding Machine

Designed for precision grinding of contour templates, the NC machine (Fig. 4.1) consists of a T-shaped base with two machine slides mounted on

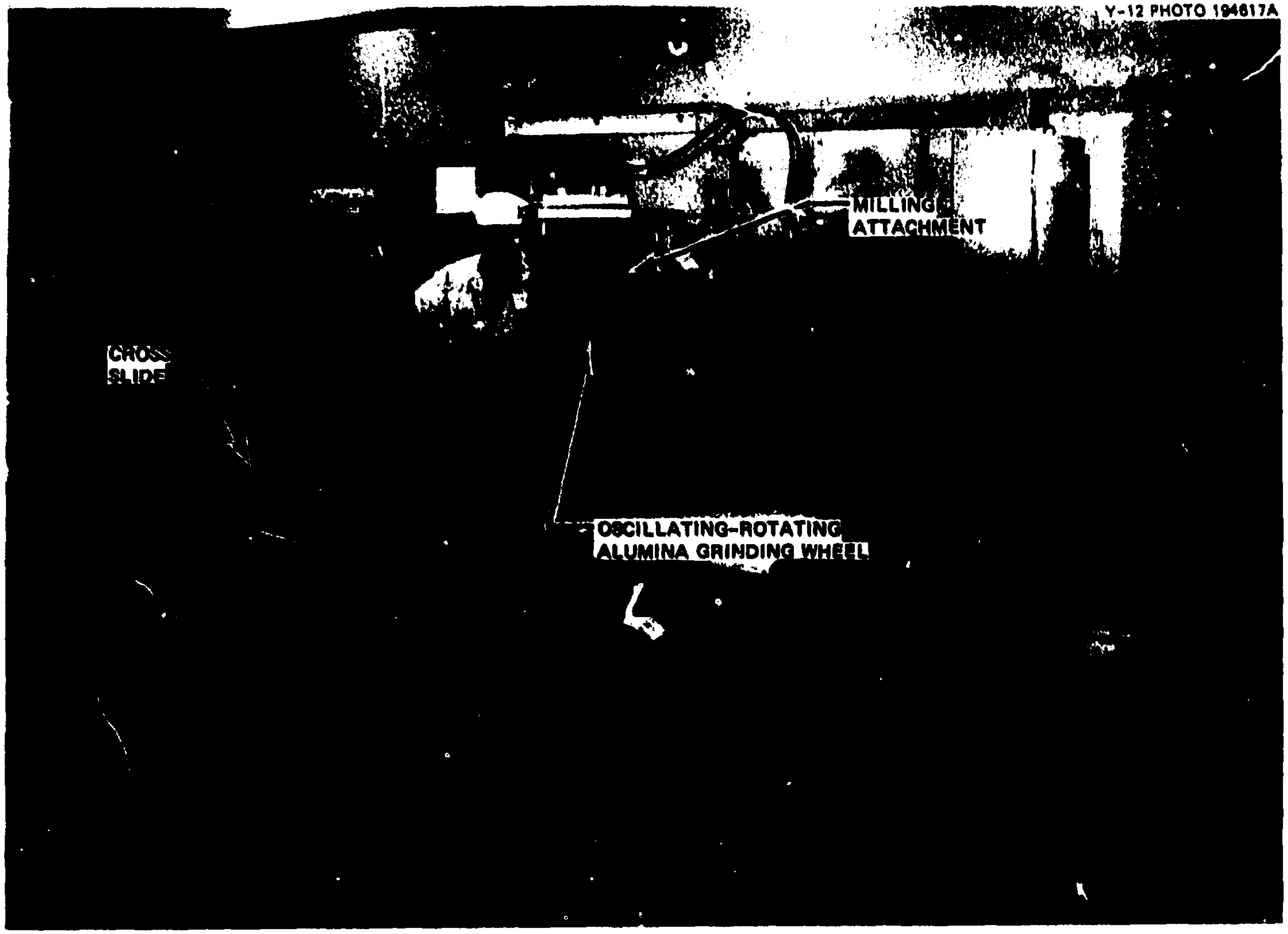

Fig. 4.1. Numerically controlled (NC) template grinding machine.

the base at right angles to each other. The slides are operated through gear boxes by ball screw and nuts driven by servo-controlled hydraulic motors. The front cross or work slide has a 137-cm (54-in.) travel; the rear or wheel-tool slide has a 71-cm (28-in.) travel.

The grinding head consists of a ball-bearing spindle for a rotating grinding wheel mounted on a vertical hydrostatic slide with an adjustable vertical oscillating stroke up to 38.1 mm (1-1/2 in.). This grinding head provides the capability to precisely cut parts with a thickness as great as the stroke length. The 50-cm-diam (20-in.) grinding wheel is a 180-grit, aluminum oxide, vitrified bond wheel with a 1.98-mm (0.078-in.) surface cutting radius dressed onto the periphery. Mounted behind the grinding wheel is a swivel-type dresser automatically operated and arranged so that the amount of wheel dressed off is automatically compensated to maintain size. The machine has been retrofitted with a vertical spindle-milling attachment mounted on the grinding head to rough mill the template blanks prior to finish grinding.

The electronic machine control unit is a Bendix Dynapath 1800 two-axis integrated-circuit tape control system. Operational control is via an eight-channel punched tape. Control information is fed to hydraulic servo-motors that drive the feed screws of the machine slides. The system has a 0.00005-mm (0.00002-in.) minimum increment and will provide traverse rates up to 76 cm/min (30 in./min).

4.3 NC Drive Tape Generation and Use

This section describes the generation of control tapes for the GCFR-CFTL FPS variable-width ribbon. The process is the same for other types of heating elements except that the length and contour of the elements are different. Longer elements may require more than the two-stage setup described here.

Tapes are generated from the contour information supplied from Eqs. (3.20) through (3.23). The NC tape program for control of the template grinding machine equipment consists of one control tape for each of the two stages of travel. The NC tapes are generated for only one side of the ribbon profile because the ribbon is symmetrical. One complete side of the ribbon is machined using stage-1 and stage-2 tapes. Ribbon stacks are then reversed on the machine, and the same two tapes are used to cut the profile on the opposite side of the ribbon stack.

Figure 4.2 shows the machine drive path for stage-1; stage-2 (not shown) is similar. Both tapes consist of a setup pass and a contouring pass, shown by the appropriate lines in Fig. 4.2. The datum is the horizontal line above the ribbon profile that is parallel to the cross or work slide of the machine. The stage-1 setup pass starts and ends at the high point of the ribbon contour. The contour pass begins at that point and proceeds left to the ribbon contour, then right to a triangular tab at the far right of the machine travel.

The NC tape for stage-1 is designed to machine more than half the contour length of the element, including the triangular tab. The tab's purpose is to establish the relationship of the second-stage tape to the program of the first-stage tape. The tab (Fig. 4.2) is a triangle with 45° angles rising from the element surface. Pickup points for the stage-2 program are on the sides of the tab, thus establishing the relationship of cross slide travel between the two programs. Because the programmed travel of the stage-2 tape overlaps programmed travel of the stage-1 tape by ~25 mm (1 in.), the tape's tool path for stage-2 will blend with the finished surface of that of stage-1. This overlap accurately establishes the main or tool slide relationship between the two program tapes.

Control of the relationship of the two sides of the heating element stack contour is by measurement across each end of the element stack,

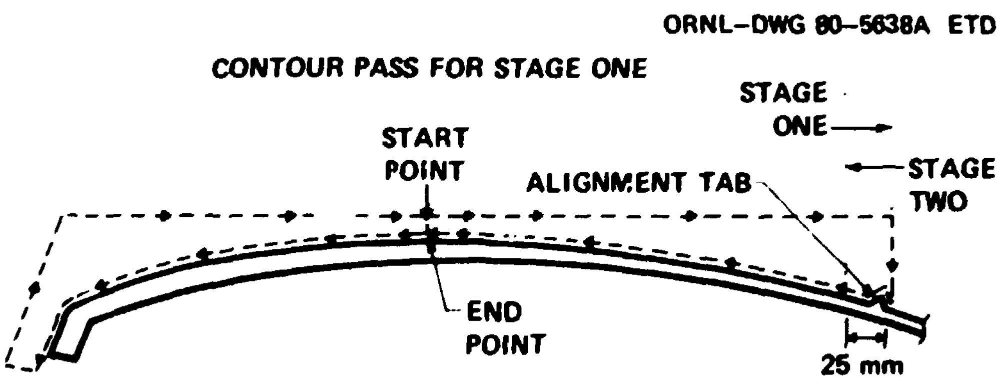

Fig. 4.2. Contour defined by stage-1 NC tape for GCFR-CFTL FPS variable-width heating element.

making a 57.13° angle (32.87° with its perpendicular) to the travel of the cross slide. Thus, the cross slide relationship to the rotated element stack is established, and, by measuring across the center of the element, the main or tool slide relationship to the rotated element stack is measured.

4.4 Process Development

The GCFR-CFTL elements are fabricated from 0.25-mm (0.010-in.) Kanthal A-1 stock placed in a stack of 15 pieces held between 2 steel plates that provide support. Figure 4.3 is a photograph of the stacked Kanthal stock being encased within the steel plates. The top plate (to left in the photo) is the reference part of the entire stack and has two 7.6-cm-long (3-in.) datum feet, premachined on one longitudinal edge located 101 cm (40 in.) from center to center and equidistant from either end of the plate.

The ribbon stock is stacked between the two steel plates flush with the edge opposite the datum feet and flush with the left end when facing the edge having the datum feet. The entire stack is then clamped in position to the front-side support fixture (Fig. 4.4) situated on the cross slide of the machine. This support fixture consists of a 9.5-mm (0.375-in.) steel plate that is 30 cm (12 in.) wide and 177 cm (70 in.) long, including the datum feet. This plate is identical to the stack top plate on one longitudinal edge and has a premachined element contour on the other edge. Toe clamps are positioned along the contour every 15 cm (6 in.).

With the stack-support fixture assembly firmly clamped into place, the program tape for stage-1 is used to define the path of a 3.7-mm-diam (0.156-in.) flute high-speed steel end mill that rough cuts the contour of the first stage of the element's front-side. The end-mill cut is set up relative to the cross slide and the tool slide, allowing sufficient stock to be removed during subsequent grinding of the stage-1 element contour. After the stage-1 front-side contour is rough cut, the cutter is moved out of position and replaced with the grinding wheel, utilizing the same program tape as for rough cutting. The stage-1 element contour

Fig. 4.3. Stack of 15 ribbons being encased within stainless steel holding plates.

Y-12 PHOTO 194473

Fig. 4.4. Front-side support fixture.

is finish ground (Fig. 4.5). Still encased in the front-side support fixture, the element stack is then moved in a longitudinal direction on the cross slide to set up for stage-2 rough-cut end milling (Fig. 4.6). The end mill then machines the second portion of the front side of the element contour in the same manner as previously described. Relationship between the cutter passes of the two tapes is maintained because the same datum surface, located on the element stack (front-side support fixture assembly), is used on each setup.

At this point in the machining process, with half of one side of the element stock finish ground and the other half rough cut, the alignment tab located at the end of the first portion of the contour (Fig. 4.6) is milled from the contour because it is no longer necessary in the machining process of the front-side element. With the second portion milling pass completed, the contour is ready for finish grinding. Final relationship between the first and second portions of the contour surfaces is established to within 0.0025 mm (0.0001 in.) by fine blending of the ground surfaces with a blue die (Fig. 4.7). This completes the grinding operation of the front side of the element contour.

At this point, the entire element stack-support fixture assembly is removed from the machine and replaced with the backup plate fixture (Fig. 4.8). The backup plate fixture consists of a top support plate similar to the front-side support fixture except that its front surface is a replica of the element contour. The bottom plate of the backup plate fixture, also with a premachined contour on one edge, extends outward from beneath the top support plate for a distance equal to the designed element width minus 50 mm (0.020 in.). Toe clamps are affixed every 15 cm (6 in.) along the contour on the plate to hold the element stack in position. To assist in in-process element width control, slots are machined in the plate in midcontour position and at each end of the contour.

The element stack front-side support fixture assembly is moved back to the machine to place the previously finished front-side element contour in position firmly against the contour of the top support plate. The toe clamps of the top support plate are tightened down (Fig. 4.9) to hold the element stack in position. After the top support plate toe clamps are secured, toe clamps on the front-side support fixture are loosened, allowing

Fig. 4.5. Stage-1 element contour being finish ground.

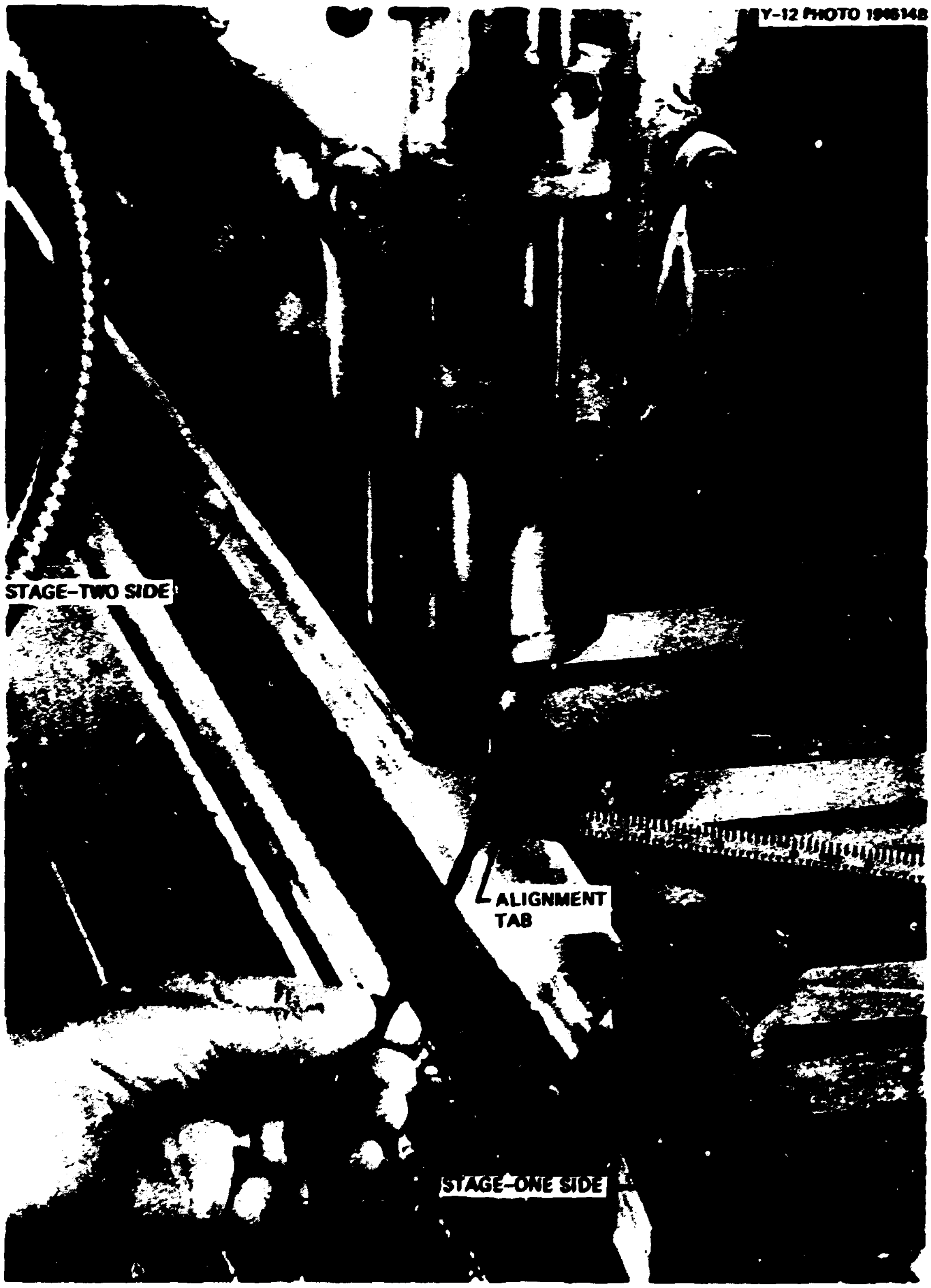

Fig. 4.6. End mill shown just past alignment tab in position to start stage-2 rough cut.

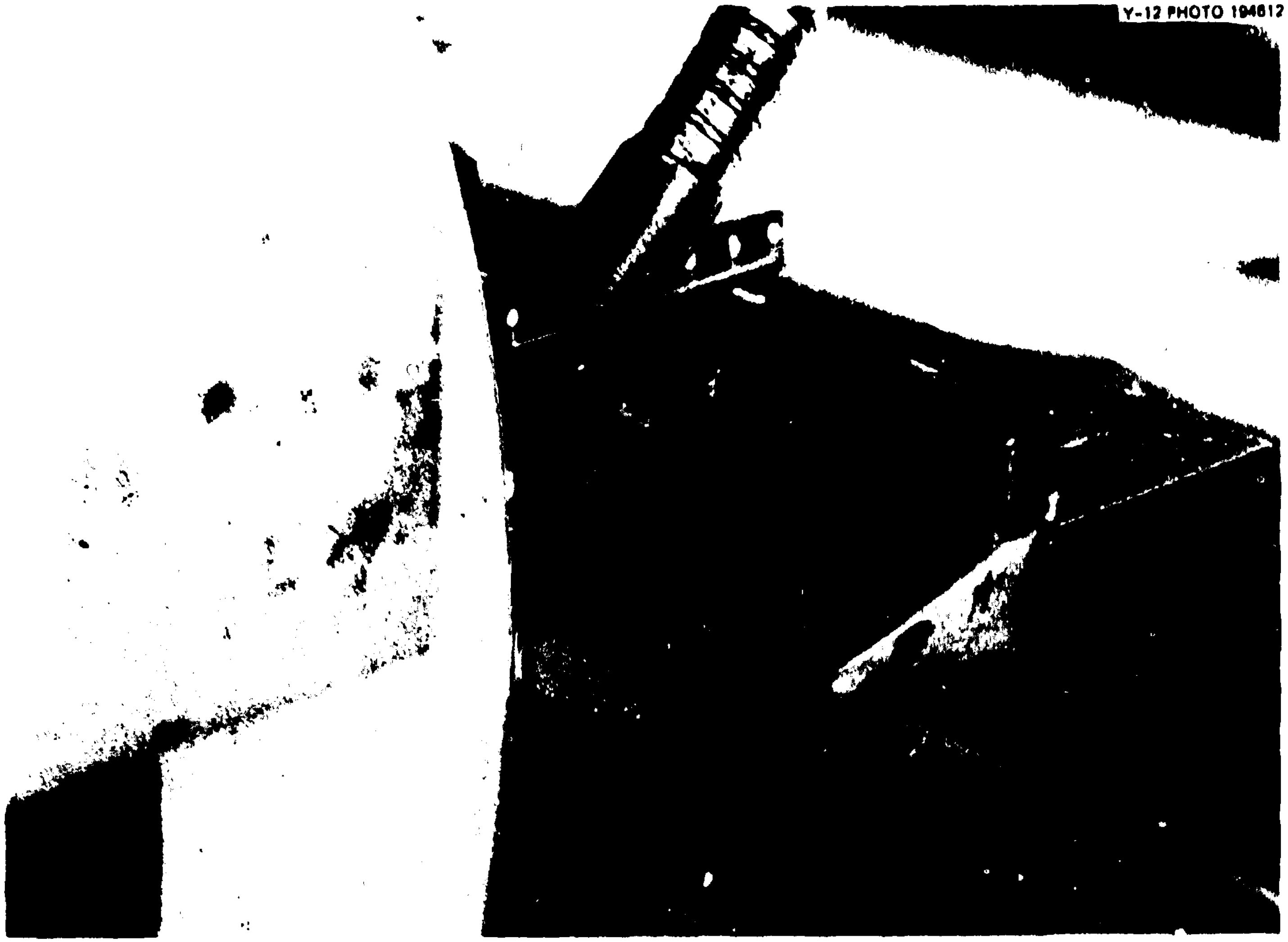

Fig. 4.7. After alignment tab is machined off, stage-1 and stage-2 contour surfaces are established to within 0.0025 mm (0.0001 in.) by fine blending with blue die.

Y-12 PHOTO 194472B

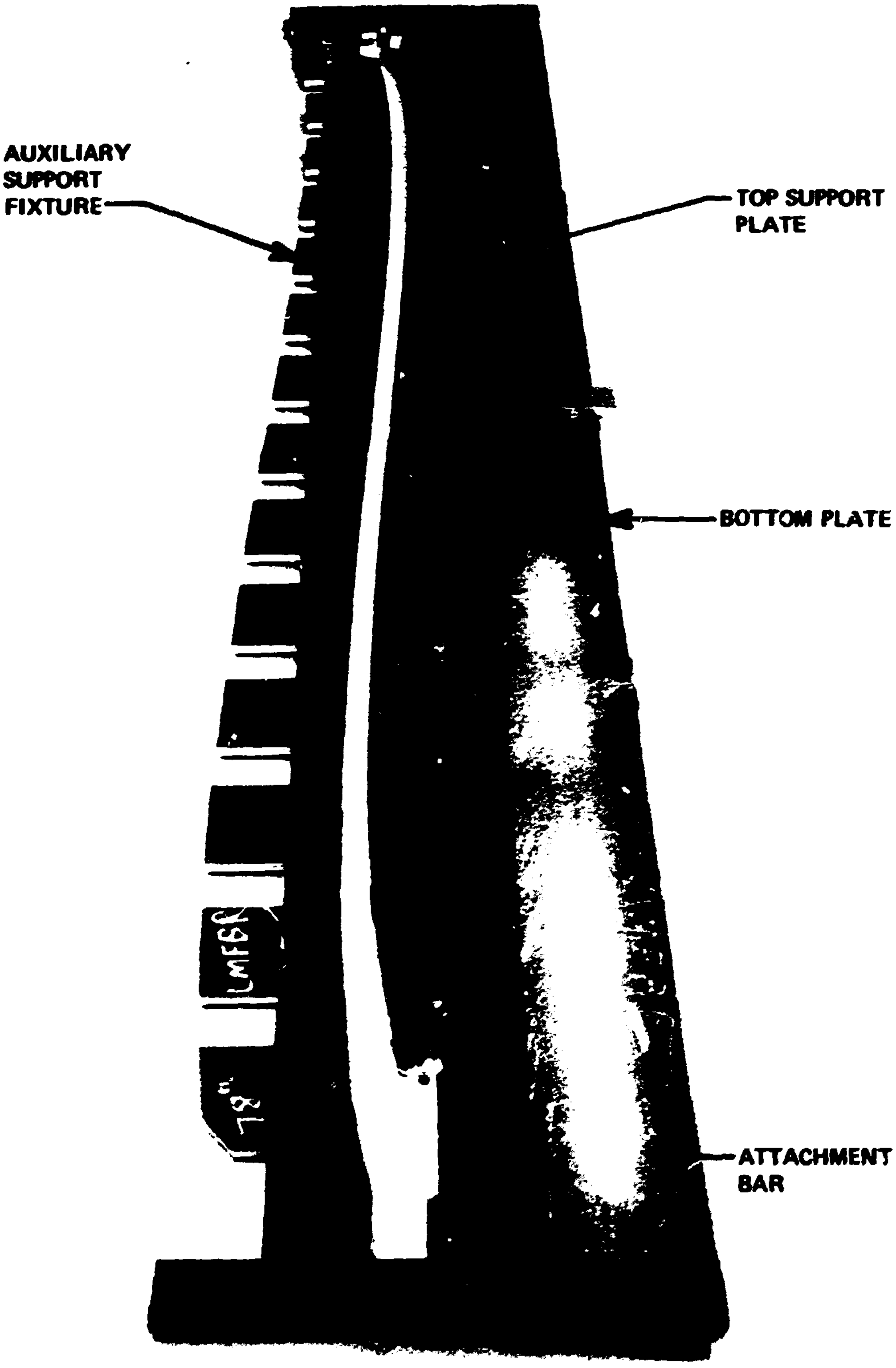

Fig. 4.8. Backup plate support fixture and auxiliary support fixture attached to each other by attachment bars at either end.

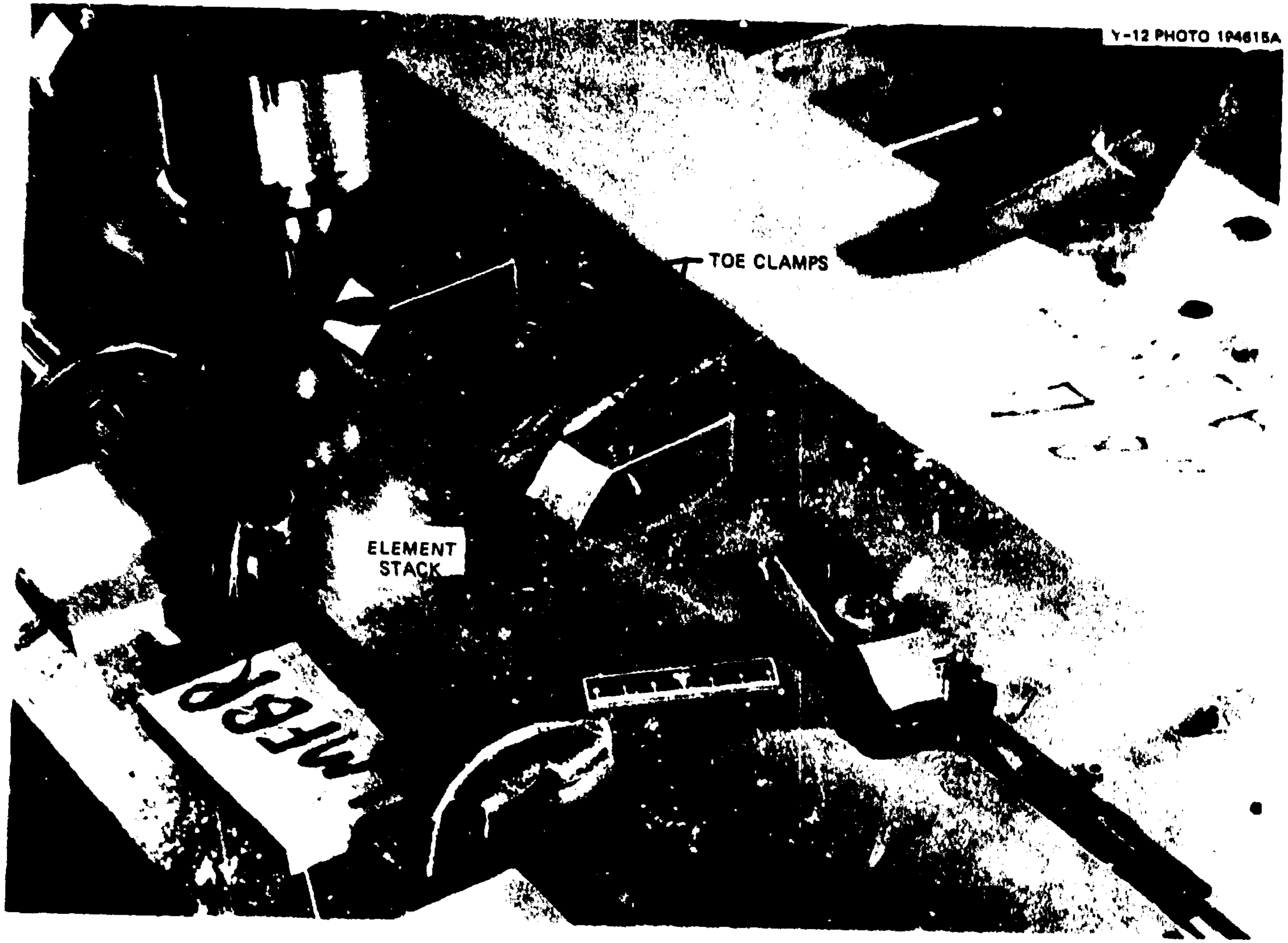

Fig. 4.9. Start of end milling of first stage of second side of element stack. End-mill cut is positioned by scribed line shown.

the fixture to be separated from the element stack and to be replaced by an auxiliary support fixture (Fig. 4.10). The auxiliary support fixture is a 15-mm-thick (0.6.5-in.) aluminum plate with the element contour machined on both solid and notched longitudinal edges. Designed to steady the element stack during the rough-milling stage of the second-side contour machining, the auxiliary support fixture is attached to the backup plate fixture by a 50-mm-wide (2-in.) by 25-mm-thick (1-in.) steel bar at each end. Bolted in position beneath the element stack, the auxiliary fixture supports it ~25 mm (1 in.) away from the backup plate fixture, allowing enough room for a milling cutter to pass between the two plates.

With the element stack nestled in the backup plate fixture and supported by the auxiliary support fixture, the first stage of the second-side contour is ready for machining. Setup positioning for the milling operation of the first portion of the contour is established on a scribed line located the width of the element away from the finished surface of the first-side contour (Fig. 4.9). Machined into the front-side contour and used for cross slide location, the alignment tab is not machined into the second-side contour. Instead, the tab's outline is scribed on top of the top plate of the element stack (Fig. 4.10). After setup is complete [allowing 1.7 mm (0.070 in.) excess stock], the first stage of the second-side is rough milled, and the entire assembly is moved on the cross slide into position for the second stage of the second-side contour milling (Fig. 4.11). Setup for slide locations is similar to that used on the front-side contour.

After completion of two rough-milling phases of the second-side contour, the element has been severed from the remainder of the stack. The stack auxiliary support fixture assembly is then unbolted from the backup fixture (Fig. 4.12) and removed from the machine, allowing the backup plate fixture (with the elements attached) to be repositioned for grinding of the first stage of the second-side contour.

Before the grinding operation, a steel tab (used for setup) is bolted to the under surface of the backup plate fixture at the end of the first portion of the contour (Fig. 4.13). A milling pass of 0.76 mm (0.030 in.) depth is then made, establishing 45° angles on the newly affixed tab.

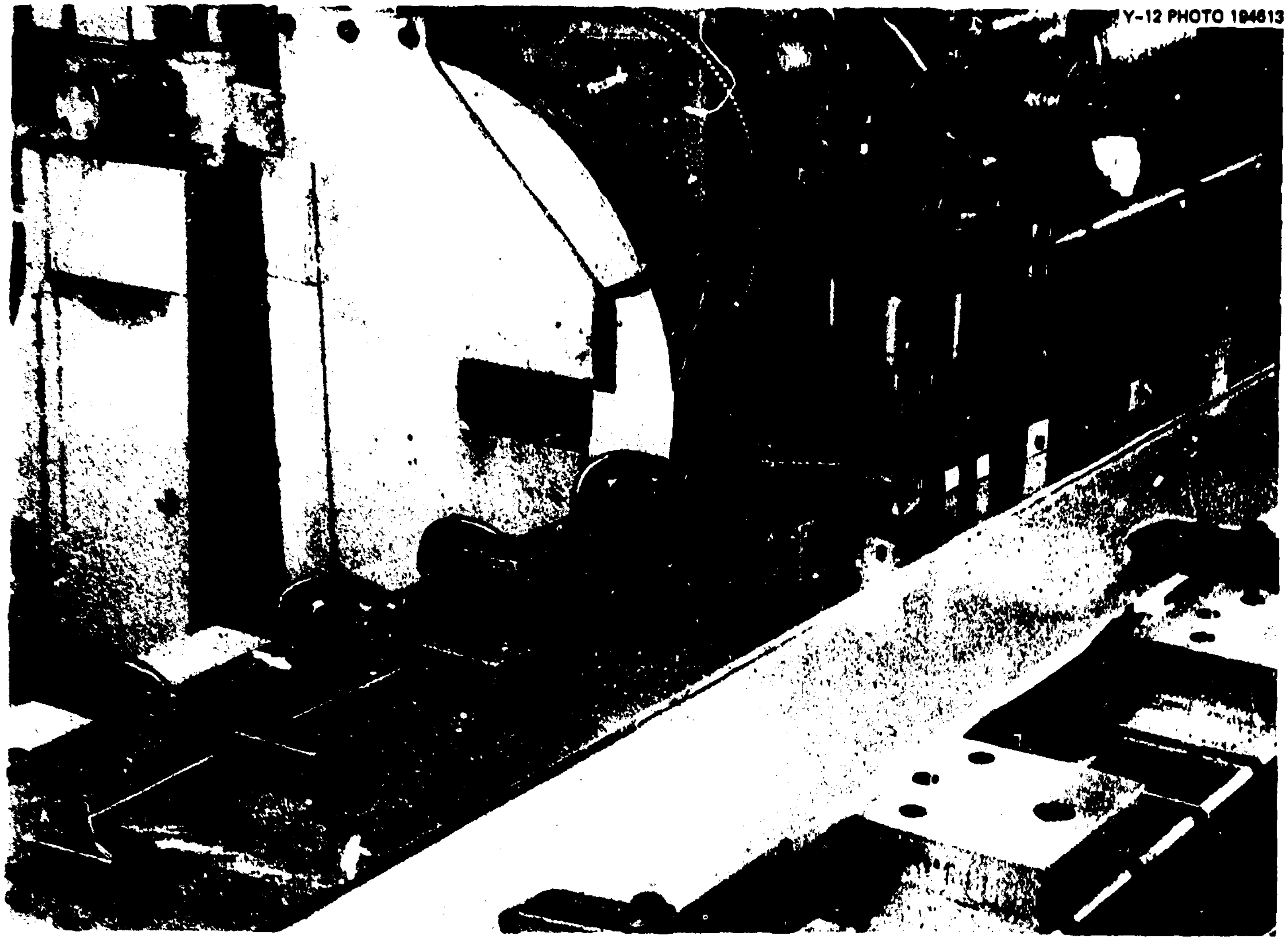

Fig. 4.10. Outline of alignment tab is scribed on top plate of element stack to reference stage-2 to stage-1 of second side.

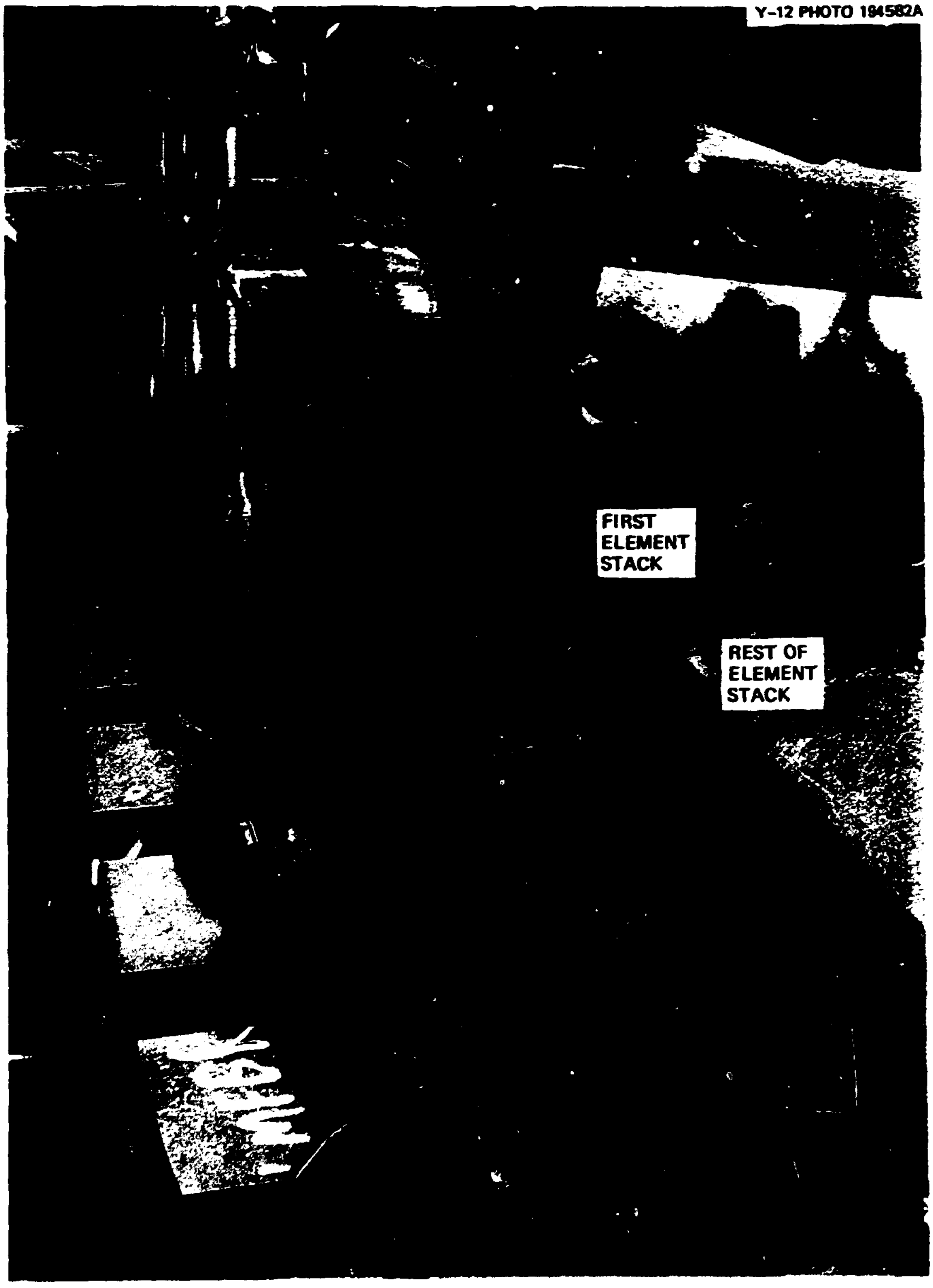

Fig. 4.11. Completion of second-stage milling of second side of element stack.

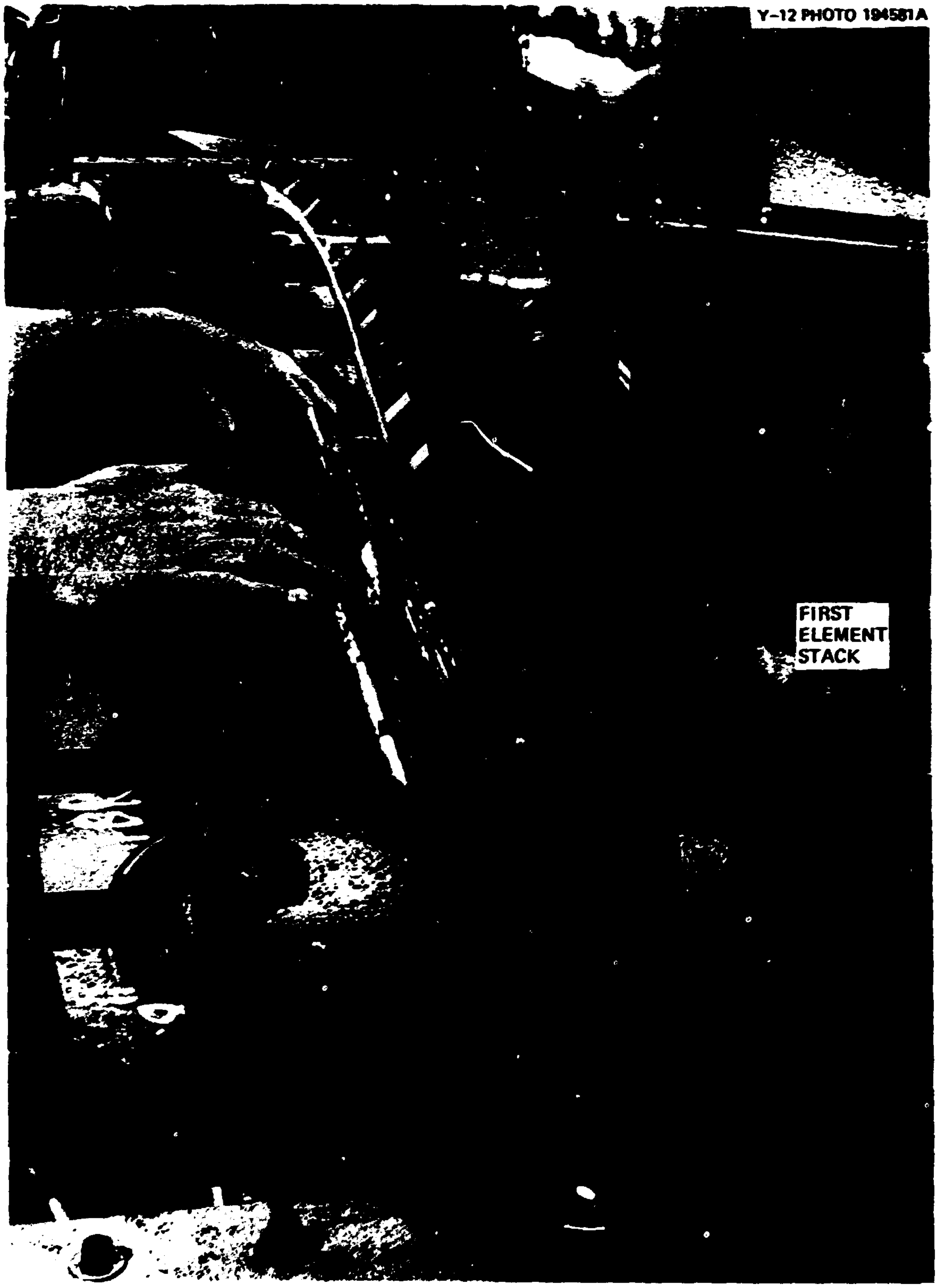

Fig. 4.12. After completion of milling passes, auxiliary support fixture is detached from backup fixture leaving first stack of machined elements ready for final grinding of their second side.

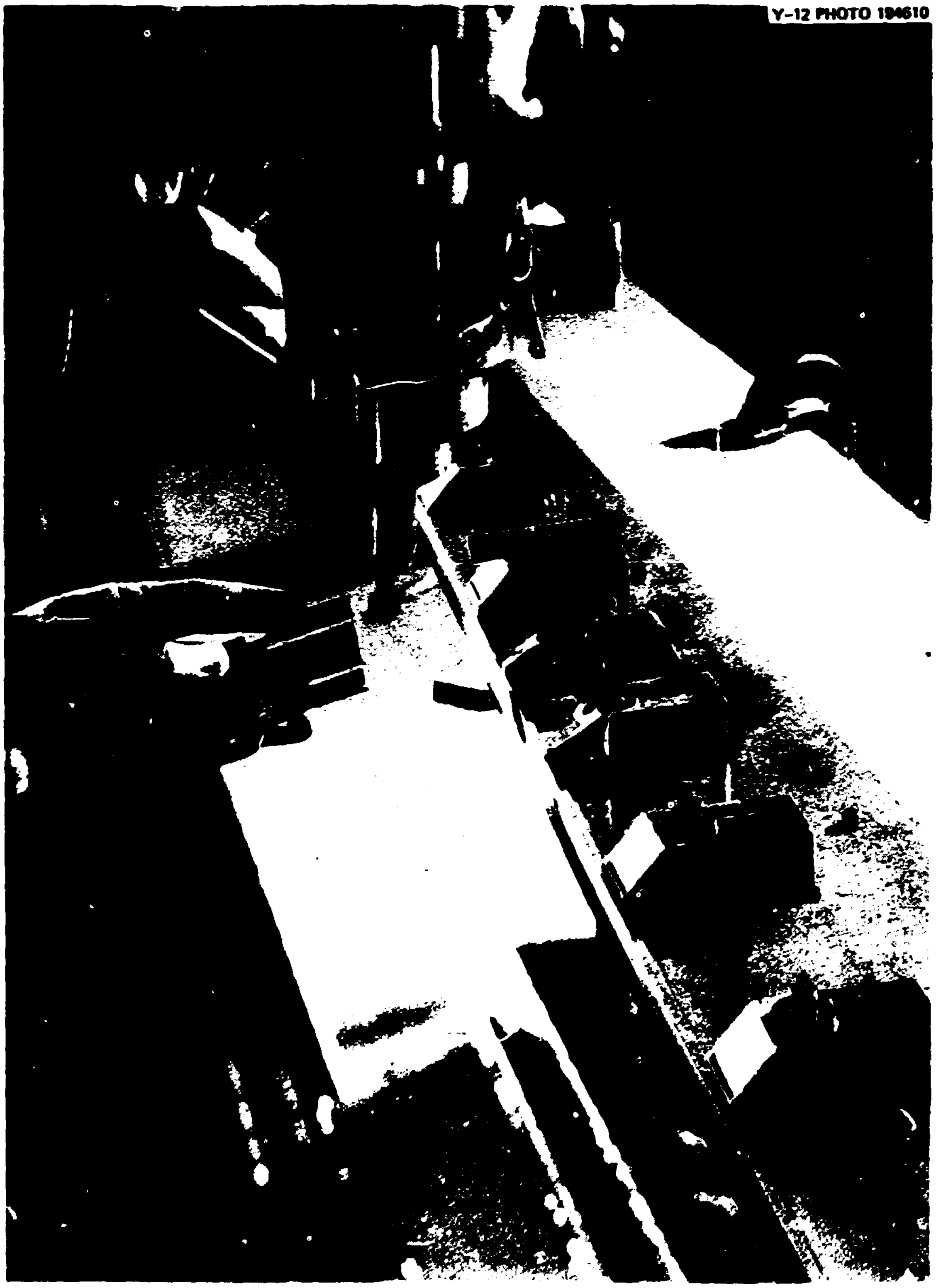

Fig. 4.13. Prior to second side, stage-1 grinding pass, a tab is bolted to support fixture. Tab is then scribed to establish stage-1 to stage-2 alignment.

Next the grinding pass is made to finish the first stage of the second-side contour (Fig. 4.14). Relationship between the second side and the finished first side of the element is maintained by micrometer measurements across the element stack at the longitudinal midpoint (Fig. 4.15) and across the starting end of the element. The final relationship between the first and second stages of the contour is again established by the overlap of the two programs for a distance of ~25 mm (1 in.). The finished surface of the first stage is coated with a blueing liquid for a distance of 25 mm (1 in.), and the two surfaces visually blend as the ground surface of the second stage appears on the blued finish surface of program No. 1. After the designed element width is achieved, the element backup plate fixture is moved on the cross slide into position for the final operation.

The setup for the second stage of the second side is made on the alignment tab, as described previously. This is followed by rough milling and the rough- and finish-grinding passes. Width control measurements are again taken at element midpoints and across the ends. The geometry of the variable-width element allows minimal correction by cross slide movement without appreciably affecting the element design width. After the design width has been achieved at the end and at the blend point of first and second stages, the machining of the 15-element stack is complete (Fig. 4.16).

The stack is then unclamped from the backup plate fixture, each element is inspected, and all burrs are removed with a 600-grit emery cloth. Using 15-cm-wide (6-in.) starting stock, 4 additional groups, totaling 75 elements, can be machined from the original stack. Four groups can be machined from 10-cm (4-in.) stock.

Figure 4.17 shows the geometry of the elements inscribed within the ribbon stock outline. Element local width and contour tolerances within 0.013 mm (0.0005 in.) have been achieved consistently. The total time to fabricate 60 elements is ~200 h, or 3.3 h/element. The NC tape generation, design, and fabrication of tooling (a one-time task for each type of variable-width element) takes ~280 h. Although the limitation on stacking probably has not been reached, larger stacks would not be practical. The

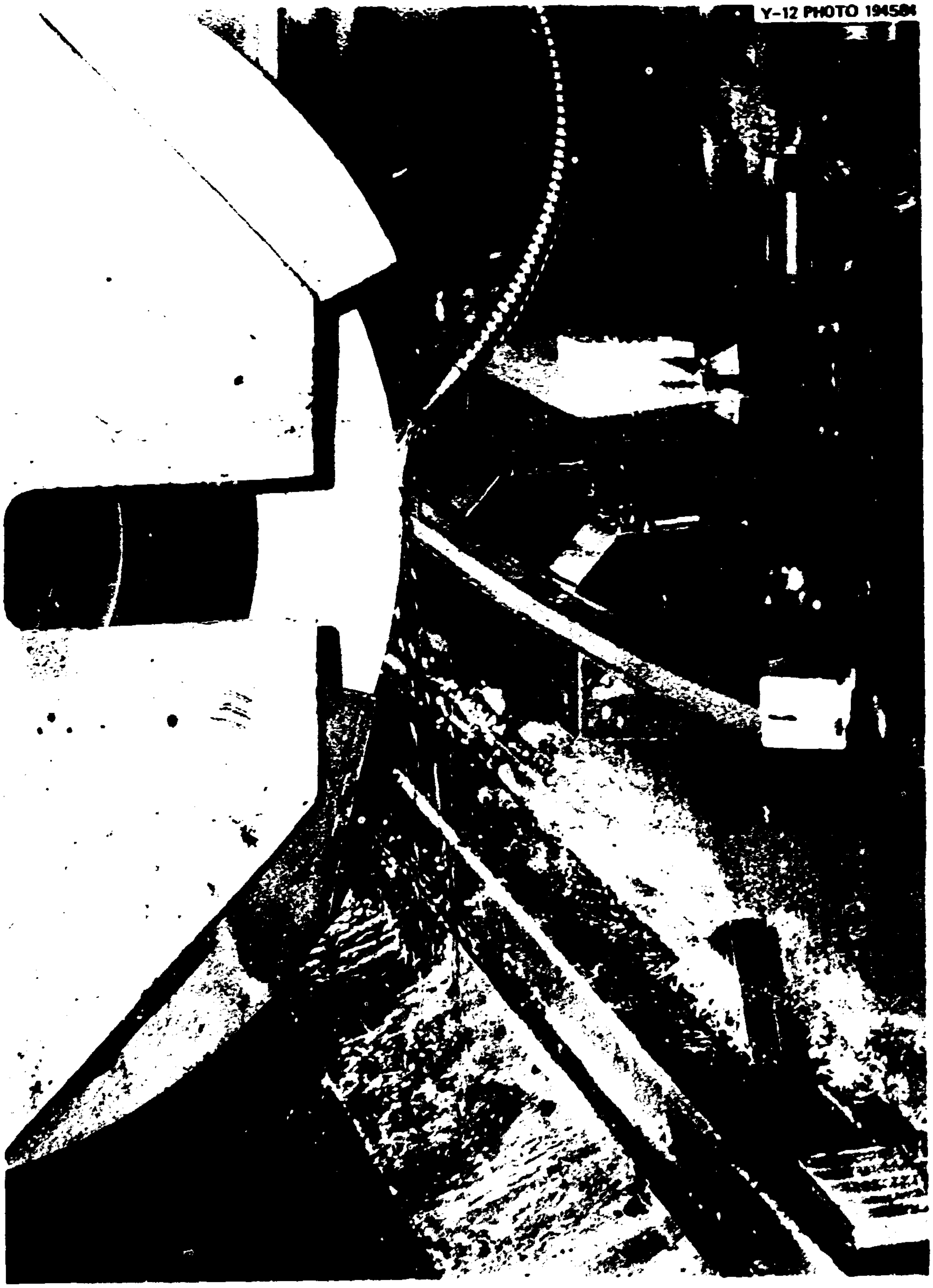

Fig. 4.14. Stage-1 grinding pass of second side is then completed.

Fig. 4.15. Ribbon design width is established by micrometer measurement of element stack at its midpoint.

Y-12 PHOTO 194665

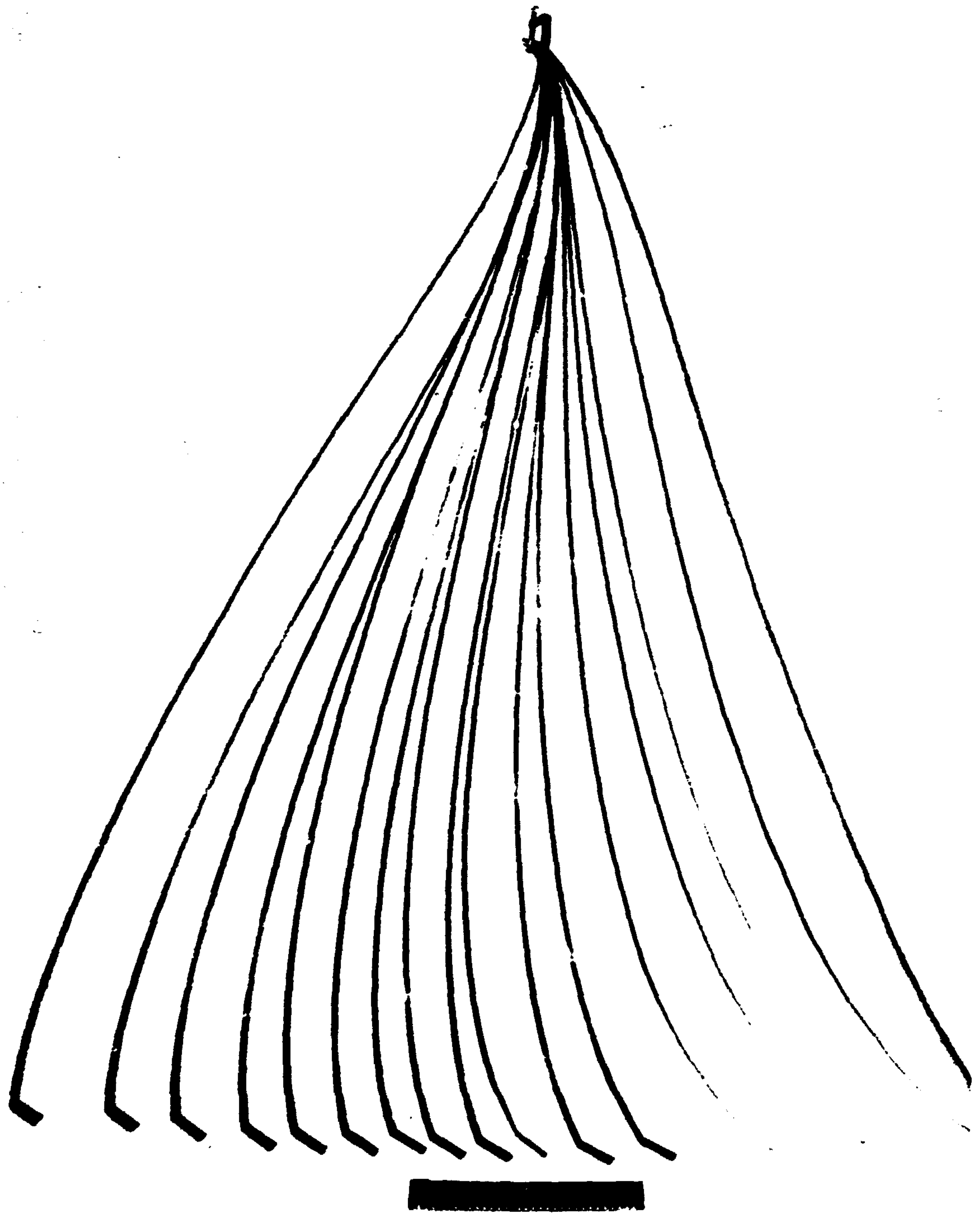

Fig. 4.16. Completed stack of 15 elements with top and bottom steel plates.

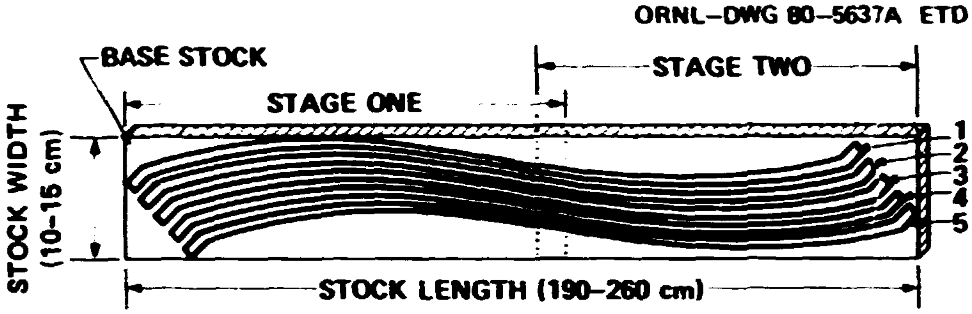

Fig. 4.17. FPS heating element geometry within ribbon stack.

machining of a greater number of elements in the stack would be achieved only with the use of special longer flute end mills. Using longer end mills would then present increased cutter pressures leading to cutter breakage and increased machining time.

44

5. RIBBON WINDING

5.1 General

The contour-ground Nichrome V or Kanthal A-1 variable-width ribbons are fo med into spirally wound coils using the method and equipment discussed here. Although development of winding techniques was accomplished for both GCFR and BRP FPSs, only the winding of GCFR coils will be described. Strips provided for winding were geometrically defined and fabricated so that, when correctly wound about an appropriately sized cylindrical substrate or mandrel, (1) a uniform gap exists between all coil turns (for those coils programmed to be wound with a gap), (2) a desired coil outer diameter is achieved, and (3) a coil of a defined finite length results.

Reproducibility of coil parameters is highly desired, this demands that a high-precision, automated winding machine be utilized. Most importantly, the precision winding process requires winding equipment that possesses a controllable variable lead rate (inches per revolution). This can be programmed to be synchronous with the contour ground strip dimensions as the strip is wound onto a properly sized substrate. The Development and Assembly divisions of the Y-12 Plant have such equipment and provided technical and fabrication support for the winding process.

5.2 Coil-Winding Machine and Associated Fixtures

The Black-Clawson four-axis NC winding machine has the required control capabilities and thus was selected to wind the coils (Fig. 5.1). This machine can filament wind a surface of revolution within a dimensional limit of 4.4 m (4 ft) in diameter by 8.8 m (8 ft) in length. Most conventional filament-winding applications require use of the four-motion axis depicted in Fig. 5.1. However, for winding of variable-width coils, only the Y-axis and θ-axis motions were required. Neither the X-axis nor the A-axis were employed. A typical coil-winding operation is shown in Fig. 5.2. For GCFR coils, a 3.68-mm-diam (0.145-in.) stainless steel rod was used as the winding substrate. This rod was ~122 cm (48 in.)

ORNL-DWG 80-5639 ETD

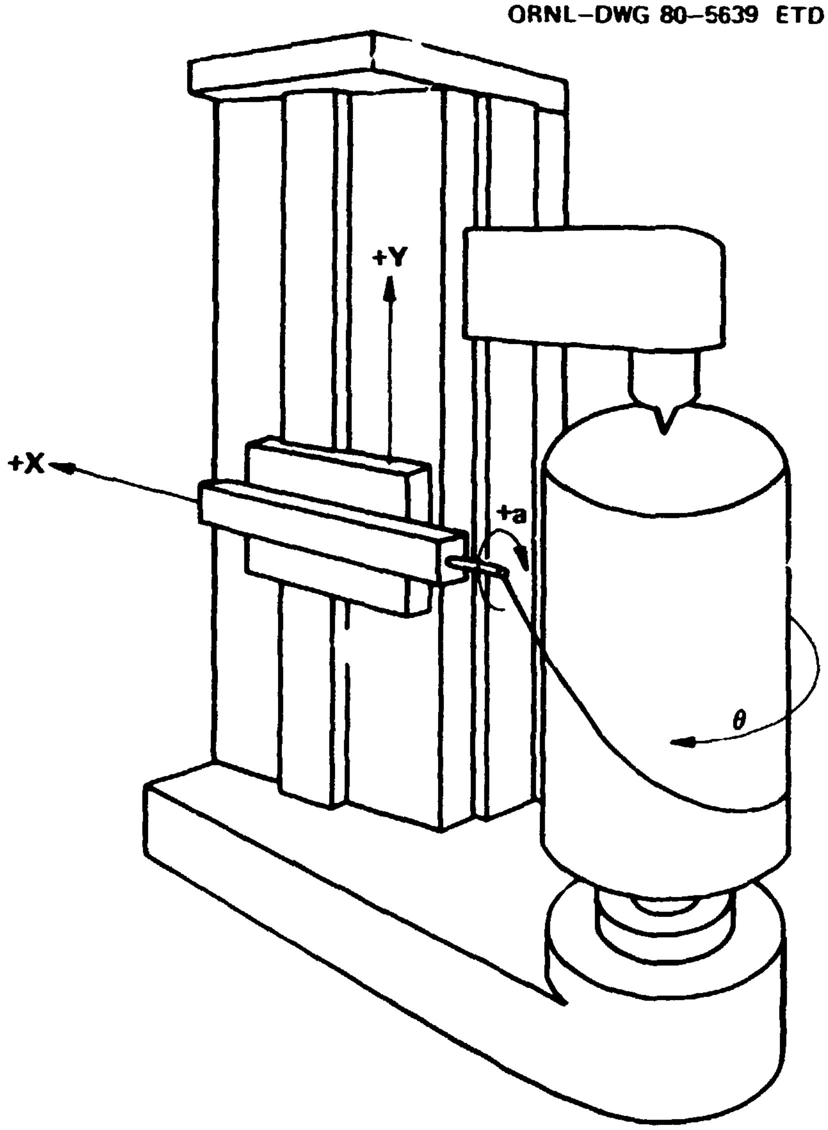

Fig. 5.1. Schematic layout of Black-Clawson winding machine.

in length and was loaded under tension between the headstock (base of m--hine) and tailstock (Fig. 5.2). Additional fixtures required to wind th. coils include a winding die mounted to the machine ram. A close-up of the headstock chuck and the coil-winding die is shown in Fig. 5.3. Figure 5.4 shows a coil being wound with a die affixed to the machine ram.

The winding is positioned by the ram so that the winding mandrel is concentric to the precision-drilled hole through the tungsten carbide insert in the body of the die (Fig. 5.4). The die is made in two sections

Y-12 PHOTO 1[illegible]102

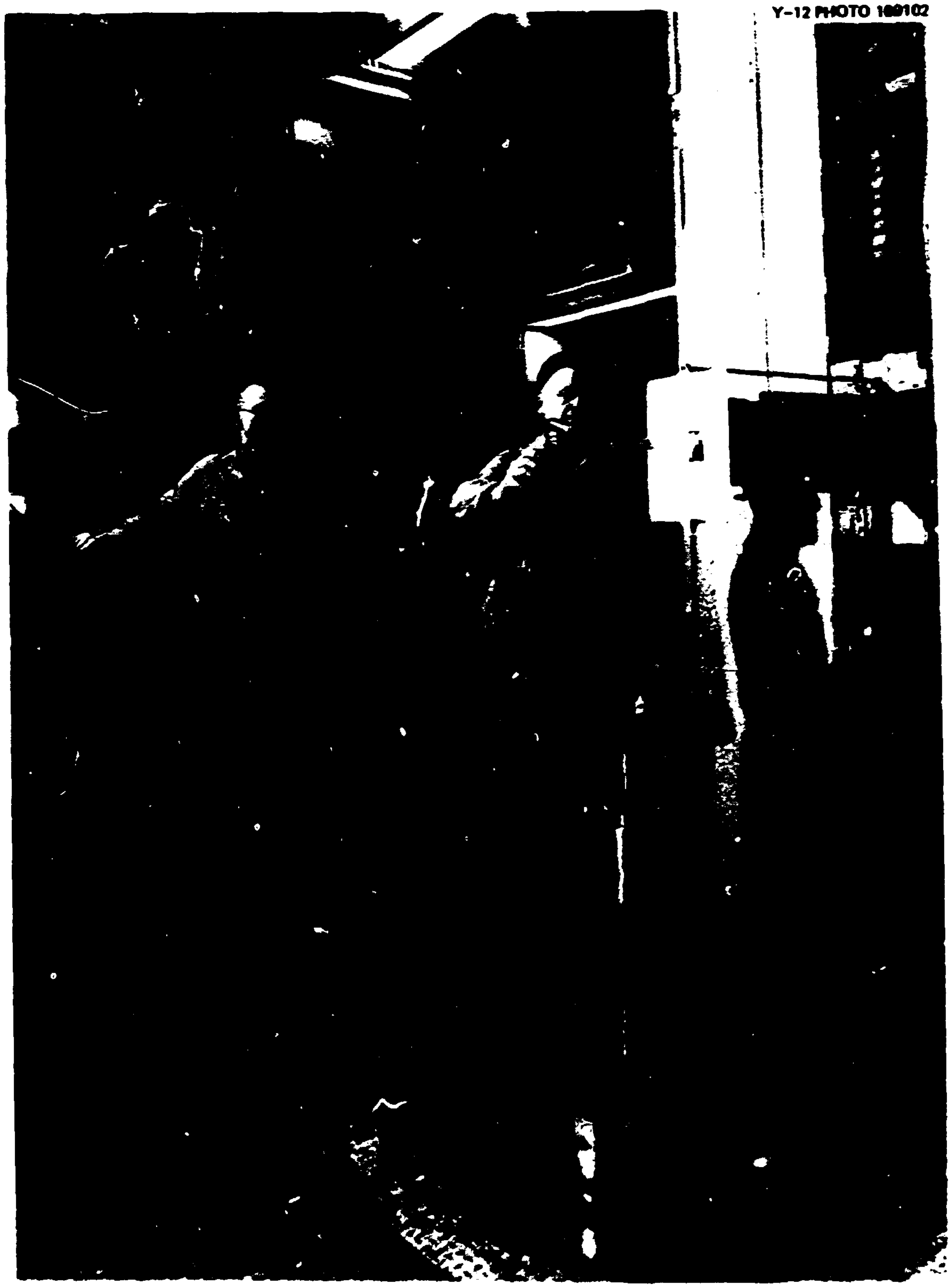

Fig. 5.2. Typical coil-winding operation.

Y-12 PHOTO 169106

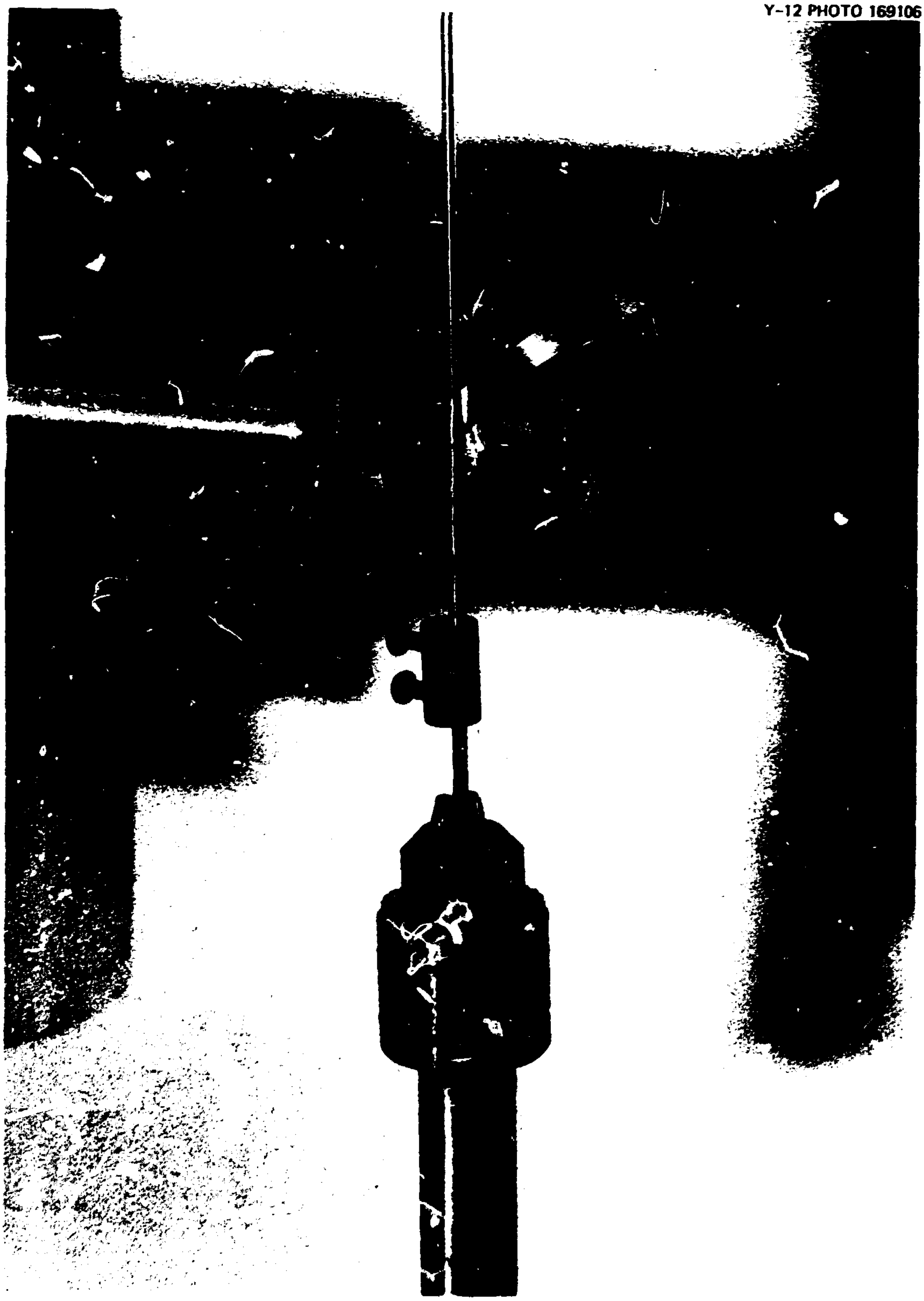

Fig. 5.3. Headstock chuck and winding die.

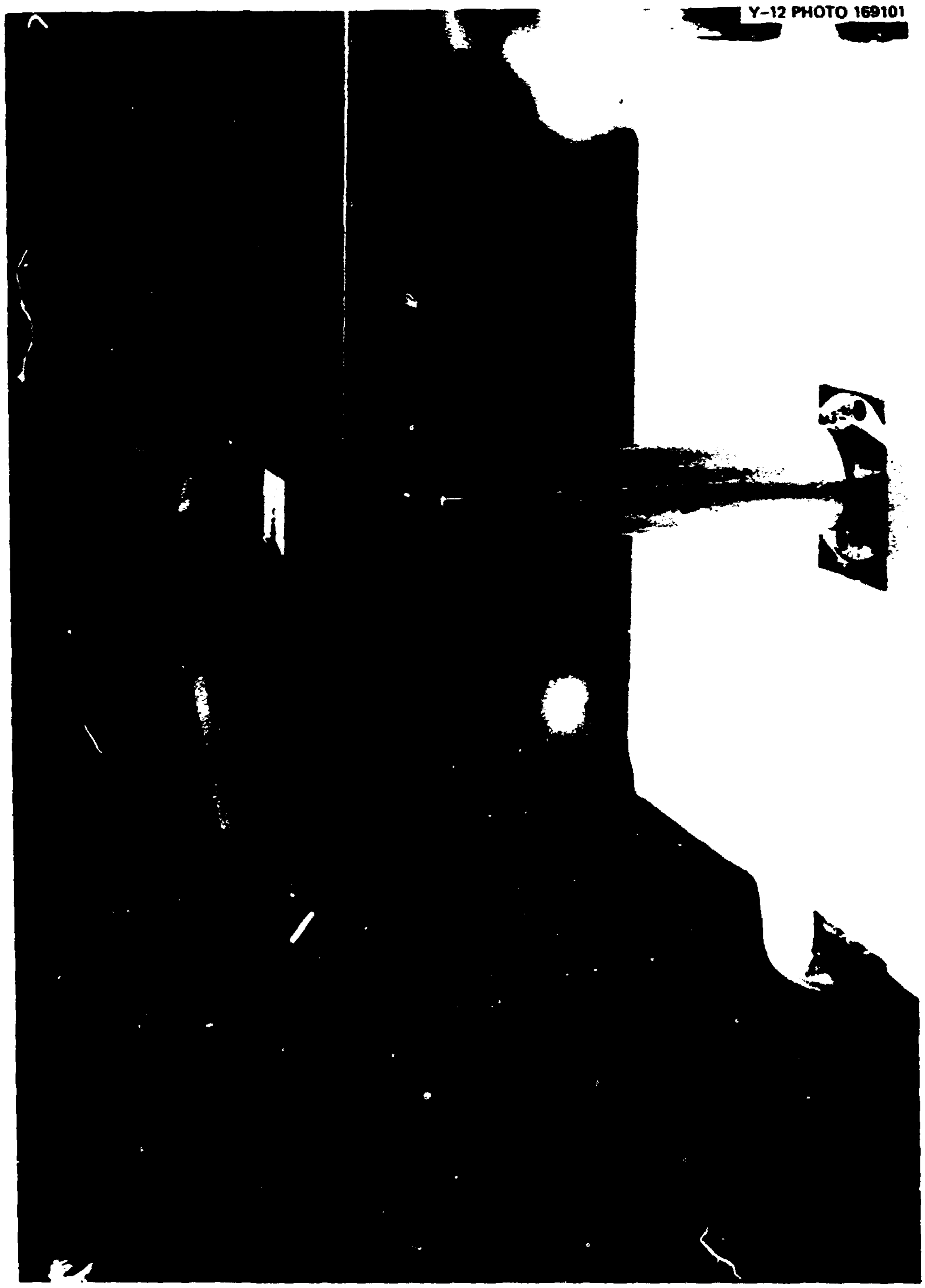

Fig. 5.4. In-process coil winding with die, held by machine ram, moving upward vertically on a rotating mandrel.

(Fig. 5.5) so that the ribbon strip can be positioned with the die body at the approximately correct feed angle prior to initiation of automatic (tape control) winding.

As evident in Fig. 5.3, the first two coil turns are manually wound and formed above the winding mandrel using modified hand tools (Fig. 5.6). After the coil is prepared for winding (as described previously), the mating half of the winding die is attached and tightened. Alignment pins are used to ensure a circular die bore when assembled.

The central bore of the die for the GCFR coils was 4.24 mm (0.167 in.). Used with a nominal 3.68-mm (0.145-in.) winding mandrel, this diameter results in a nominal radial clearance of 0.025 mm (0.001 in.) used with a 0.25-mm-thick (0.010-in.) Kanthal A-1 or Nichrome V strip. A ribbon-strip feed slot is machined on one-half the die body with the feed angle at 22.5°, measured with respect to the horizontal plane (Fig. 5.5). This is required to allow the ribbon to feed freely into the working bore of the die and also to maintain automatically the proper feed angle at the wound coil midpoint.

5.3 Coil-Winding Program Design

Design of the winding program is accomplished using a relatively simple computer code that requires an effective mandrel diameter and the contour definition of the ribbon strips as input.

The die speed is programmed to vary in proportion to the element width perpendicular to the mandrel axis w_v. Winding parameters are adjusted to satisfy the equation

$$\frac{w_v + G_v}{\pi} = D_{eff} , \tag{5.1}$$

where G_v is turn-to-turn gap dimension perpendicular to the mandrel axis and D_{eff} is effective winding diameter. For winding with no gap,

$$D_{eff} = \frac{w_v}{\pi} ,$$

where D_{eff} equals OD − t ideally but may vary from that value somewhat

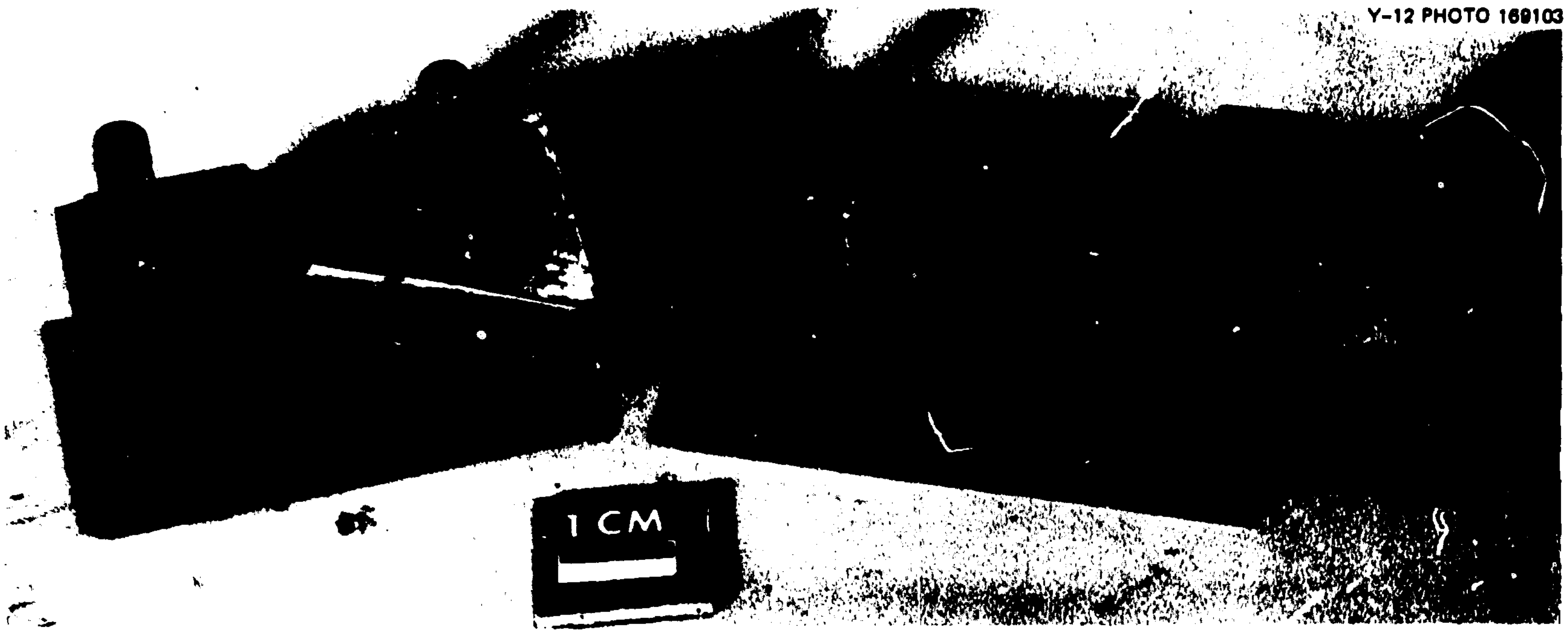

Fig. 5.5. Typical winding die.

Fig. 5.6. Tooling used to form strip ends for initial attachment to winding mandrel.

if tensile and compressive stresses on the ribbon material are not similar in value. For the GCFR coils, the effective diameter used for final winding pattern definition was 3.94 mm (0.155 in.).

Ribbon contour data input is the x,y information calculated from Eqs. (3.20) to (3.23). Output from this code includes parametric winding information for analysis and a machine control manuscript converted to punched cards for further computer processing to generate the machine control tape. These data are used as parametric input for the winding program. The winding program is designed to wind the coil incrementally by calculating a rotary displacement between successive points of the input contour definition that will wind the defined length of ribbon onto the mandrel. Included in the information calculated is (1) the incremental lead rate (TURNS/CM) of the winding program, (2) the coil turns (INCREMENTAL REVOLUTION) between successive points of the contour definition, and (3) the TOTAL REVOLUTIONS (coil turns) required to wind the contoured strip to the prescribed length using input data.

As indicated previously, only two machine axes are programmed — the vertical motion of the ram (Y) and the rotary motion of the headstock (θ). The machine is programmed to maintain a uniform rotational speed that results in a variable vertical speed consistent with the defined variation in ribbon width at respective points of the contour definition.

For the simplest case, the rotational speed is adjusted so that the Y-axis die movement will wind with the turns touching (i.e., no gap or overlap). However, as the die travels up the mandrel, winding forces cause the mandrel to twist. In addition, mandrel diameter variations and/or heating element mechanical property variations cause further perturbations that manifest themselves as errors in the Y-axis die location. Mandrel twisting or element elongation causes the true winding length to be less than programmed length, thus causing gaps between turns and excess element material at the end of the winding operation.

Several steps were taken to reduce or compensate for these errors. The die was designed so that its inside diameter was 0.05 mm (0.002 in.) larger than the mandrel and element outside diameter; a lubricant was used to reduce friction, and centerless ground molybdenum or swaged, hardened stainless steel mandrels were used in winding. Centerless grinding greatly reduces diameter variations, and the increased torque modulus of hardened stainless steel or molybdenum (when necessary) reduces mandrel twisting. Additional iterative modifications to the winding pattern were required to correct for mandrel twist and to achieve the desired degree of coil symmetry.

To alleviate the problem of empirically adjusting the software to correct for hardware deficiencies, additional tooling was designed and installed on the winding drive mechanism. This mechanism tied the headstock to the tailstock so that the winding mandrel was driven from both ends. This additional tooling was effective in permitting fabrication of more symmetrically wound coils with minimal empirical software adjustment.

Coils with diameter uniformity of 0.125 mm (0.005 in.) and length (as well as gap) tolerance variations of about 10% are now easily wound. Process and material variations preclude further improvements in tolerances. However, coils of this quality are more than sufficient for use in FPS after receiving a final touch-up operation described in the next section.

6. WOUND-RIBBON PROCESSING AND INSPECTION

6.1 General

Final winding of the variable-width ribbon produces a helical coil with dimensional and electrical characteristics very close to those desired. However, material properties and winding parameter variations make it impossible to obtain the dimensional tolerances required for use of the coils in FPSs. For example, coil springback after winding is 0.25 to 0.5 mm (0.010 to 0.020 in.) depending on (1) winding die tolerances, (2) mandrel size and mechanical properties, (3) ribbon material, and (4) local width of the ribbon being wound. Additionally, variations in gap spacing on the order of 0.25 mm (0.010 in.) are unavoidable.

Thus, determining a method of providing final touches to the coils was necessary to obtain the very close tolerances needed for FPS fabrication. Further, inspection methods that accurately indicated the condition of the ribbons were needed.

The chemical composition and resistivity of the raw material and the thickness of the strip from which the ribbons are to be cut are specified in the purchase order and certified upon receipt. Ribbon contour is closely controlled during machining. The remaining properties critical to our use are total element resistance, diameter and length of the wound coil, and thermal profile of the finished coil under transient conditions. The first two properties are determined by in-process checks that are easily accomplished using available equipment. During the development of fabrication techniques, the checks are needed to provide feedback to control dimensional tolerances of the coil and maintain the quality once the process is in use. Thermal profile evaluations are conducted with special equipment to help determine the effects of dimensional variations on the profile and to provide information on defects introduced during FPS fabrication that affect the profile.

6.2 Final Touches and In-Process Inspections

The winding operations introduce cold-work into the coils, thus increasing their rigidity. Unfortunately, the operations also deform the windings by (1) making their outer surface concave, (2) roughening the surface somewhat, (3) causing gap variations, and (4) setting the turns at a diameter that is often unpredictable and varies with the width of the turns. These difficulties can be corrected by introducing a swaging operation into the coil fabrication process.

Prior to swaging, the coils are tightly wound on a hard stainless steel mandrel with the turns touching. Both ends are attached to the mandrel, one with a clamp and the other by spot welding. The coils are then carefully swaged to lock them into this configuration. After swaging, the coils are removed from the mandrel. Swaging supplies additional cold-work to the coils to (1) lock the turns in place, (2) set the diameter, (3) remove the concavity introduced by winding, and (4) decrease the surface roughness. Depending on the element material and configuration, a springback of 0.025 to 0.076 mm (0.001 to 0.003 in.) is predictable and easily corrected by proper sizing of the swaging mandrel.

Additional cold-work put into the coils by swaging makes them rigid and mechanically similar to a spring. Gaps between turns are then produced simply by stretching the coils about 5 to 10% of their length. The coils do not plastically deform under these conditions; thus, gaps between turns no longer depend on the local material yield stress and are quite uniform.

After swaging and dimensionally inspecting the coils' outside diameter with a micrometer, the coils are cleaned in a vapor degreaser and cut to the exact length required. Equal amounts are cut off each end to maintain a symmetrical chopped-cosine profile.

The electrical resistance of the coils is closely monitored throughout their fabrication. Each coil is assigned a serial number after being machined. Resistance is measured and recorded at that time as well as after (1) winding, (2) swaging, (3) assembly into an FPS, (4) swaging of the FPS, and (5) annealing of the FPS. The data collected are used to determine the optimum value of the design resistance based on the final coil resistance needed in the FPS.

Resistance values are measured with a system that uses a dc power supply, a digital voltmeter, a 1-Ω resistor calibrated to 0.01%, and associated leads and switching equipment. Heating elements are connected to the dc power supply in series with the 1-Ω calibrated resistor. Voltage across the resistor is monitored, set to 1.0000 V (1.0000 A through the circuit), and then monitored across the elements. This reading in volts corresponds to the exact resistance in ohms. Contact resistance is eliminated using this method. Repeatability was demonstrated to be better than 0.5%.

6.3 Transient Thermal Profile Evaluation

An important aspect of coil fabrication is the evaluation of its transient temperature profile before assembly of the coil into the FPS sheath. The evaluation must answer the question, "How well does the heat distribution produced by the coil fit the design criteria?" Because we were interested in a test for the coils that described heat distribution, a logical method was infrared scanning. Although inspection by infrared scanning of FPSs has been used for some time,[7] it was not used for inspection of any central heating element until development of the variable-width coil for production of a cosine temperature distribution. These investigations were done during the testing of several types of coils. Although specimens used for development of the test procedure differ in design, they do not introduce uncharacteristic variables.

The nature of the infrared scanning camera dictates that test objects must be held in a horizontal position, and the need for near-perfect alignment of the flexible coil posed a few installment problems. For example, the coil could not be suspended between two points without sagging. This meant that a stiff supporting arbor, electrically insulated from the coil, was needed. A Pyrex glass rod would have served very well, but common rod diameters were not suited to a close fit with the coil's inside diameter. The most acceptable arbor was made from a brass rod enclosed by shrinkable tubing. The brass rod was swaged to an outside diameter about 0.25 mm (0.010 in.) smaller than the inside diameter of the coil. When the shrinkable tubing was reduced to a tight fit on the brass rod, the final diameter allowed the arbor to be smoothly, but snugly, inserted into the coil.

Initial infrared scanning was accomplished with the coil in its normal relaxed length. Also, because of a concern for the inability to completely remove the coil, flat black paint normally applied to adjust the surface emissivity to ~1.0 was not used. Figure 6.1(a) shows the temperature profile of a BRP coil at the end of 6 min with a 25-W input. The signal on the left ordinate of the scan is from a temperature reference source set at 70°C (158°F). However, the actual peak temperature of the coil is higher than 70°C (158°F) because the emissivity of the coil material is considerably less than unity. Baseline for the scan is room temperature — about 23°C (73°F).

Figure 6.1(b) shows the smoothing effect when the coil is stretched. Here the coil is elongated about 2.5 cm (1 in.) and is close to its final condition in an FPS. Power and heating time are the same as for Fig. 6.1(a). Note the disappearance of the hot spot to the right of the coil's center. Stretching resulted in much more uniform turns-per-inch distribution because of the previous cold-work in the coil.

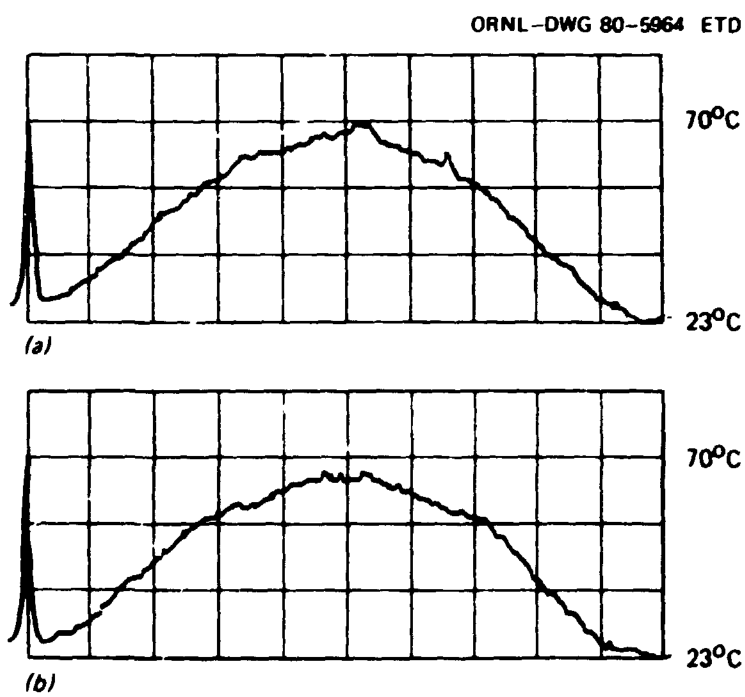

Fig. 6.1. Temperature profile shown by infrared scan of (a) relaxed and (b) stretched BRP coil at the end of 6 min with 25 W applied.

Because the nonuniformities in the temperature profile could be the result of nonuniformity of emissivity, it was desirable to paint the element to adjust the surface emissivity to ~1.0. To ensure easy removal of the element from the mandrel after the test, efforts were turned to the development of a paint removal method. The paint used is readily soluble in ethyl alcohol, and immersion of the coil in the alcohol with agitation by ultrasonic action served to thoroughly remove the paint. Final cleaning of the inside surfaces was by swabbing with alcohol-saturated pipe cleaners, while the outside was wiped with alcohol-saturated gauze.

A second BRP coil was chosen for tests to show the effects of nonuniform emissivity. Figure 6.2(a) shows the temperature profile of the unpainted stretched coil at 6 min with 25 W. Figure 6.2(b) shows the same coil painted and the obvious effect of improved emissivity on the smoothness of the profile. Also, the time has been reduced to 1 min with the same applied power for the apparent temperature to reach the level of the reference at 70°C (158°F).

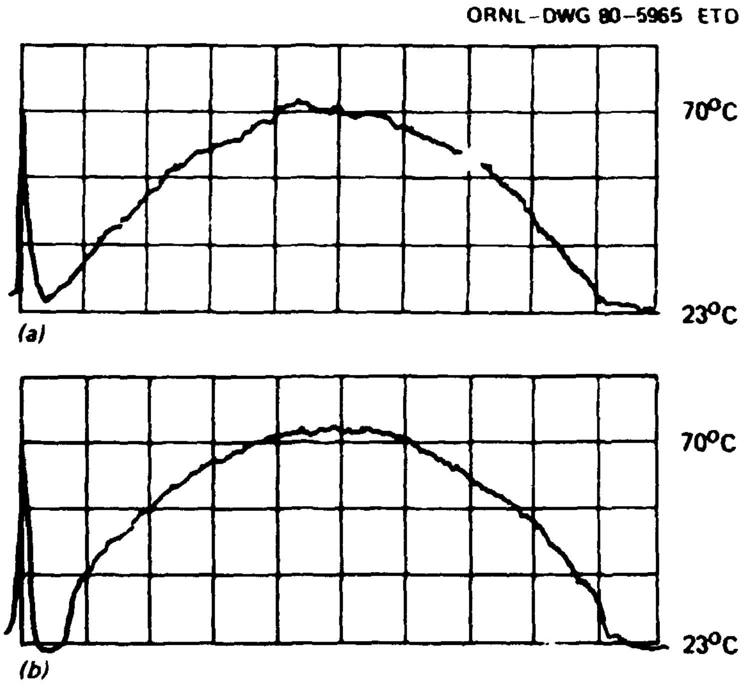

Fig. 6.2. Temperature profile shown by infrared scan of BRP coil (a) stretched but not painted and (b) stretched and painted to unify emissivity.

Infrared tests on the FPS indicated that high-power—short-time tests would describe the coil's heat production uniformity better than the low-power—long-time tests, because the amplitude or pertubation was higher and there was less time for profile "smoothing" because of axial conduction. The coil chosen for this investigation was one for the GCFR FPS and was to provide a chopped-cosine temperature profile. The added sensitivity of the short-time transient test can be seen when comparing Fig. 6.3(a), which shows the temperature profile for the low-power—long-time test where 60 W was applied for 1 min, with Fig. 6.3(b), which shows how the coil anomalies are accented by the high-power—short-time test where 1 kW was applied for 1 s.

Finally, if a very detailed analysis of a coil's performance is desired, the sensitivity of the infrared test can be increased by moving the coil closer to the camera and by reducing the camera sweep angle. Sweep angles of 10 and 25° are available. Normally, the distance between

ORNL-DWG 80-5966 ETD

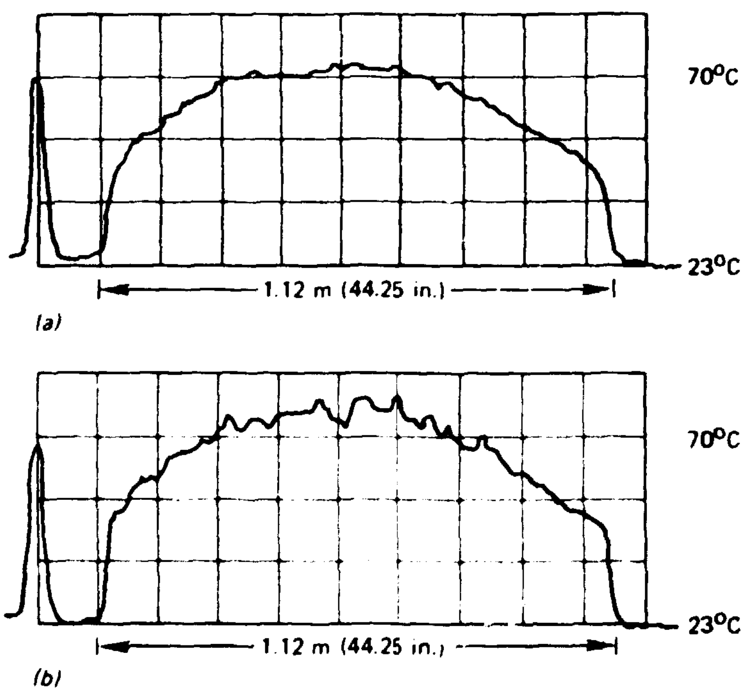

Fig. 6.3. Temperature profile shown by infrared scan of GCFR coil stretched, painted, and at (a) low power (60 W) for 1 min and (b) high power (1 kW) for 1 s.

camera and test object is set so the camera scans a path slightly longer than the test object at the 25° sweep angle. Figure 6.4(a, b, and c) shows infrared scans of a coil that was supposed to have a flat temperature profile with a uniform 2.76 turns/cm (7 turns/in.) over a 91.4-cm (36-in.) length. Obviously, an area existed where the turns were faulty, and the figures show how sensitivity is increased to the point where heat production from individual turns in the faulty area can be observed.

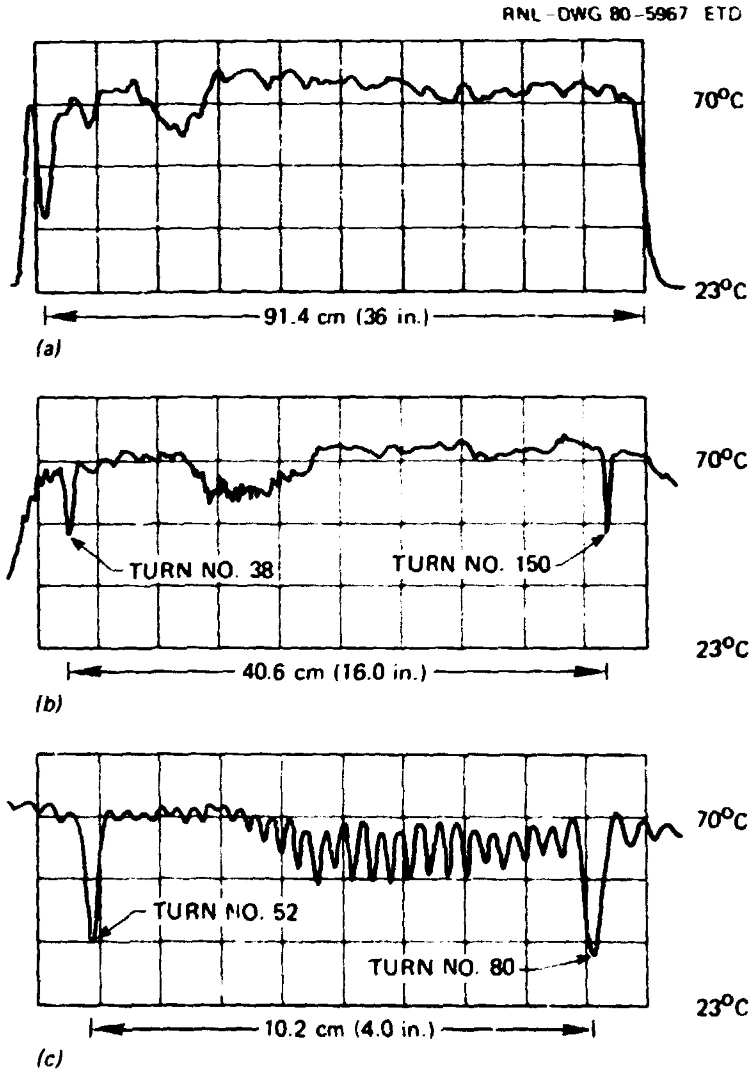

Fig. 6.4. Temperature profile shown by infrared scan of const⸗ ›t turn coil stretched, painted, and at 3.4 kW for 1 s with a camera-to-coil distance of (a) 236 cm (93 in.), 25° sweep angle; (b) 84 cm (37 in.), 25° sweep angle; and (c) 46 cm (18 in.), 10° camera sweep angle.

Once these techniques for evaluation of the coil transient profile were established, both the method and tolerances established by swaging the coils to set this diameter and the gaps were apparently sufficient. Variation in the coil diameter of more than ±0.025 mm (0.001 in.) were easily measurable. Defects causing gap variations that affected the transient thermal profile were obvious both on visual examination and by measurement of the gaps of stretched coils. A properly swaged coil exhibited gap variations (for a given width and winding angle) of no more than 0.05 mm (0.002 in.).

Infrared scan evaluations of the same coil, before and after fabrication into an FPS, helped to establish realistic operational inspection criteria for the coils and to determine the effect of defects on the final FPS transient profile.

Figure 6.5 compares infrared scans of part (a) a completed coil and part (b) a completed FPS using the coil of (a). A discontinuity in the coil gaps, causing an abrupt decrease in the turns per centimeter of about

ORNL-DWG 80-5575 ETD

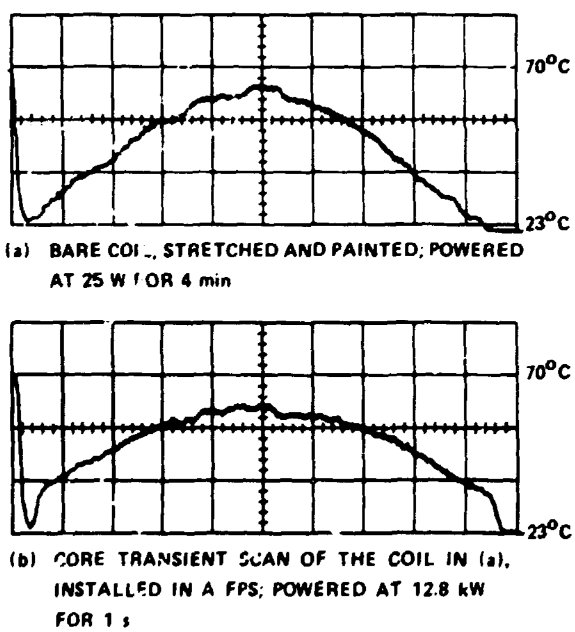

Fig. 6.5. Temperature profile shown by (a) a completed coil stretched and painted and at 25 W for 4 min and (b) same coil in a BRP FPS core transient scan at 12.8 kW for 1 s.

10% just to the right of the center of the cosine profile, was inadvertently put there during swaging. This defect is clearly discernible in both the bare coil and completed FPS. The coil profile of Fig. 6.5(a) is also accurately reproduced in Fig 6.5(b).

These data indicated that a 4-min steady-state scan of a stretched coil gives good correlation with the 1-s transient infrared scan of the completed FPS, although more detailed coil profile information is possible using high-power transient and close-up narrow range scans (as mentioned previously).

The final measure of transient performance of an FPS is obtained from a transient infrared scan. Figure 6.6 shows (a) steady-state,

ORNL-DWG 80-5969 ETD

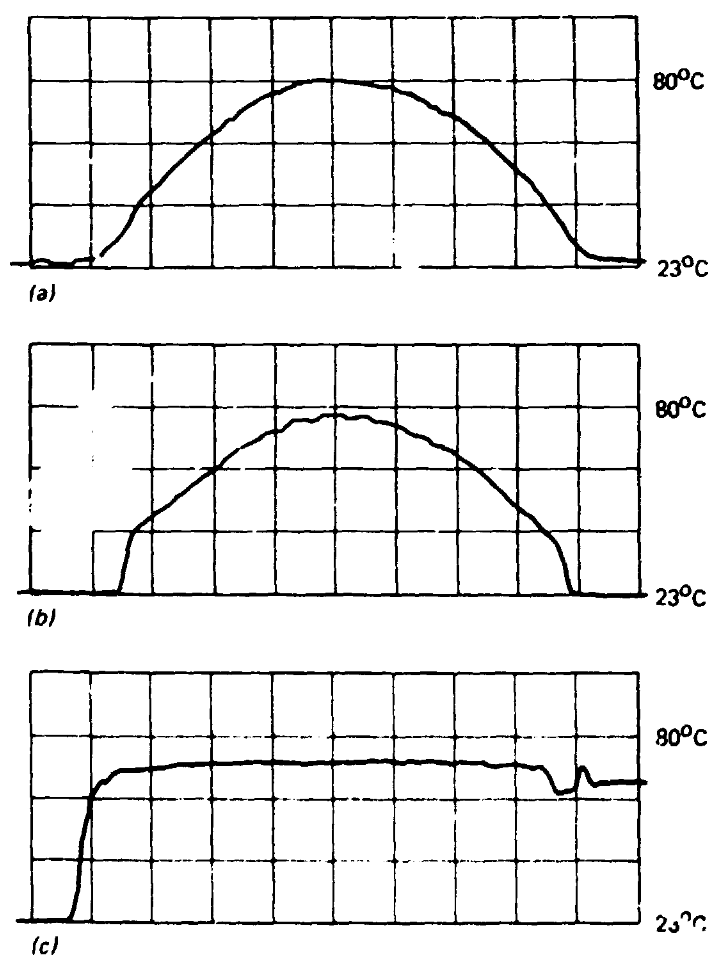

Fig. 6.6. Infrared scans of BRP fuel pin simulator: (a) core steady state, (b) core transient, and (c) clad transient.

(b) core transient, and (c) clad transient infrared scans of a BRP FPS that has been fabricated with a variable-width ribbon heating element. The core transients are obtained by applying power to the heating element and scanning the clad with an infrared camera; the clad transient is obtained by applying power to the clad before scanning it. Heat is transferred outward to the clad surface in the first two cases and inward to the FPS in the latter case. Variations reflect differences in radial heat transfer at different axial positions. For transient infrared scans, power is applied to the FPS for slightly more than 1 s, but at the 1-s instant the temperature profile of the clad is captured by the scanning system instrumentation and displayed as shown.

The core transient infrared scan profile is representative of the transient operation of the FPS, because it is at a relatively high power (~12 kW) with a ramp rate [50°C/s (90°F/s)] representative of operational tests.

7. CONCLUSIONS

Variable-width ribbon heating elements have been successfully fabricated for use in BRP and GCFR FPSs. This effort was accomplished through the cooperation of two ORNL and three Y-12 divisions: the ORNL Engineering Technology and the Metals and Ceramics divisions, and the Y-12 Development, Assembly, and Fabrication divisions.

Design of variable-width ribbons is based on a mathematically derived equation for the chopped-cosine profile. The design takes into account the synchronous variation of the local ribbon width with the winding angle, so the cross section (and therefore local heat generation) can change essentially independent of turn-to-turn spacing.

Once determined, the ribbon profile is machined on an NC template grinding machine to a local width and contour tolerance of better than 0.5%. Ribbons are wound into coils using a Black-Clawson four-axis filament-winding machine. The coils are then swaged, cleaned, cut to length, dimensionally inspected, and infrared scanned prior to use.

Infrared scan evaluation techniques were determined as part of the effort. Transient infrared scans of coils indicated that a coil outside diameter tolerance of ±0.025 mm (±0.001 in.) and coil gap variations of 0.05 mm (0.002 in.) were acceptable from a transient thermal profile standpoint. Infrared scans were used to correlate thermal inspections of the bare coil to those of the completed FPS. It was determined that a 25-W 4-min powered scan of a bare coil accurately reflects the 1-s transient infrared scan used to evaluate FPSs, while high-power—short-time scans are even more sensitive.

While maintaining a variable profile, the coils fabricated with very small gaps between turns were subsequently installed successfully in sophisticated FPSs using a precise FPS fabrication technology based on cold-pressed BN preforms. The elements were then successfully operated as components of THROS Bundle 9 FPS, THORS Bundle 12 FPS, and GCFR—CFTL Bundle AG-1 FPS prototypes.

REFERENCES

1. W. E. Baucum, R. E. MacPherson, D. L. Clark, and R. W. McCulloch, *State of the Art Fuel Pin Simulators for LMFBR Out-of-Reactor Safety Tests — Status Report*, ORNL/TM-5889 (September 1977).

2. P. A. Gnadt, R. E. MacPherson, and R. W. McCulloch, *Fuel Pin Simulators for Sodium Boiling Tests in the THORS Facility*, ORNL/TM-6688 (April 1979).

3. P. A. Gnadt, A. H. Anderson, N. E. Clapp, C. W. Collins, B. H. Montgomery, and R. D. Stulting, *An Update of the THORS Facility — A High-Temperature Sodium Test Facility*, ORNL/TM-7121 (May 1980).

4. Uri Gat and P. R. Kasten, *Gas-Cooled Fast Reactor Program Annual Progress Report for Period Ending December 31, 1977*, ORNL-5426 (August 1978).

5. Uri Gat and P. R. Kasten, *Gas-Cooled Fast Reactor Program Annual Progress Report for Period Ending December 31, 1978*, ORNL-5560 (August 1979).

6. D. L. Clark and T. S. Kress, U.S. Patent No. 3,912,908, *Electric Cartridge-Type Heater for Producing a Given Non-Uniform Axial Power Distribution* (Oct. 14, 1975).

7. W. A. Simpson, Jr., S. D. Snyder, and K. V. Cook, *Infrared Inspection and Characterization of Fuel-Pin Simulators*, ORNL/NUREG/TM-55 (November 1976).